

IPCC氣候變遷第五次評估報告(第一工作小組)導讀講座

IPCC CLIMATE CHANGE 2013: THE PHYSICAL SCIENCE BASIS

# Observations in atmosphere, surface, ocean and cryosphere

Chia Chou

Research Center for Environmental Changes, Academia Sinica



- 由結合多組獨立產製的資料所計算出的全球平均陸地和海洋表面溫度的線性趨勢，顯示1880至2012年間，暖化程度為 $0.85 [0.65–1.06]^\circ\text{C}$ 。根據資料中長度最長的一組資料，1850–1900年和2003–2012年兩段時期間的平均溫度，增加了 $0.78 [0.72–0.85]^\circ\text{C}$
- 在資料量足以進行區域趨勢計算的最長區間（1901–2012），幾乎全球的地表或海表都經歷了暖化。

# 全球近地面氣溫(陸地)

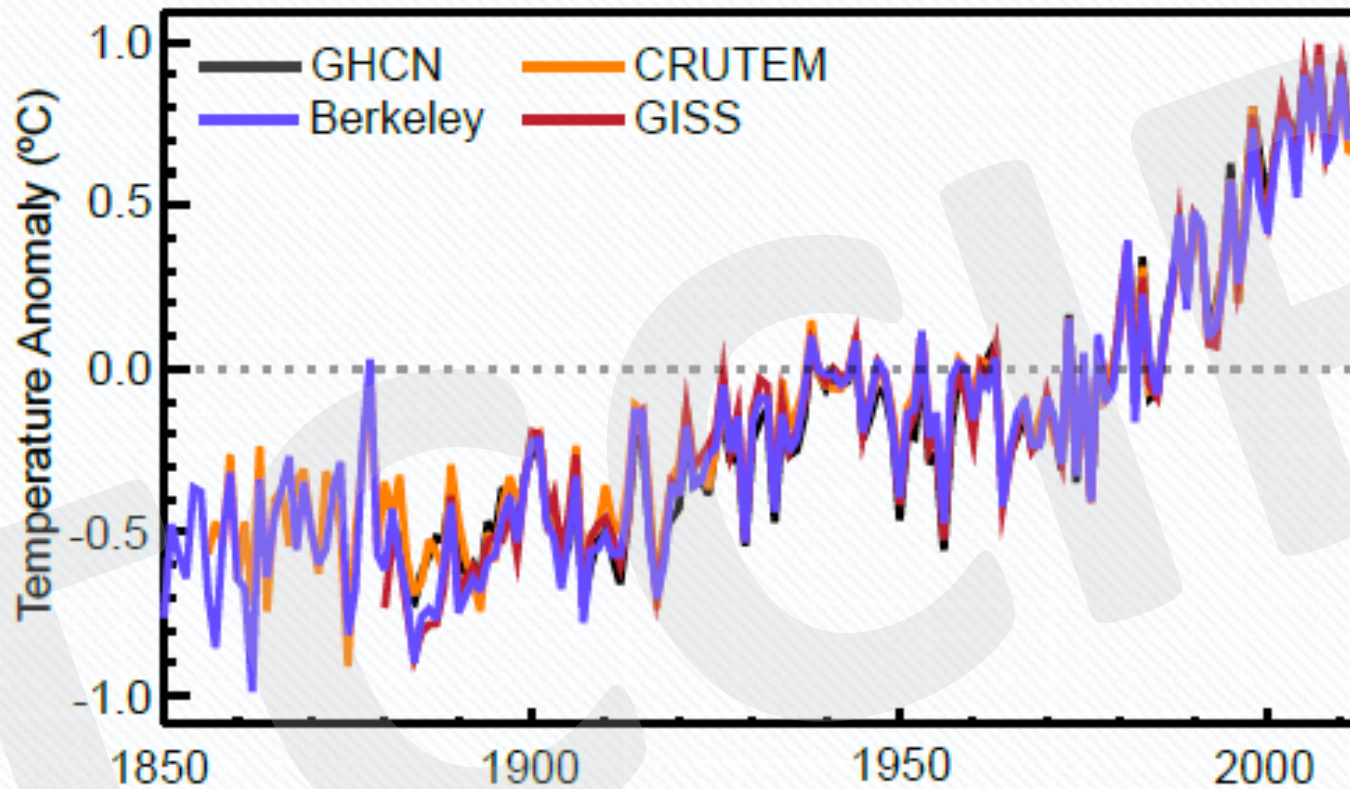


**Figure 2.14:** Global annual average Land-Surface Air Temperature (LSAT) anomalies relative to a 1961–1990 climatology from the latest versions of four different datasets (Berkeley, CRUTEM, GHCN and GISS).

# 全球海水表面溫度

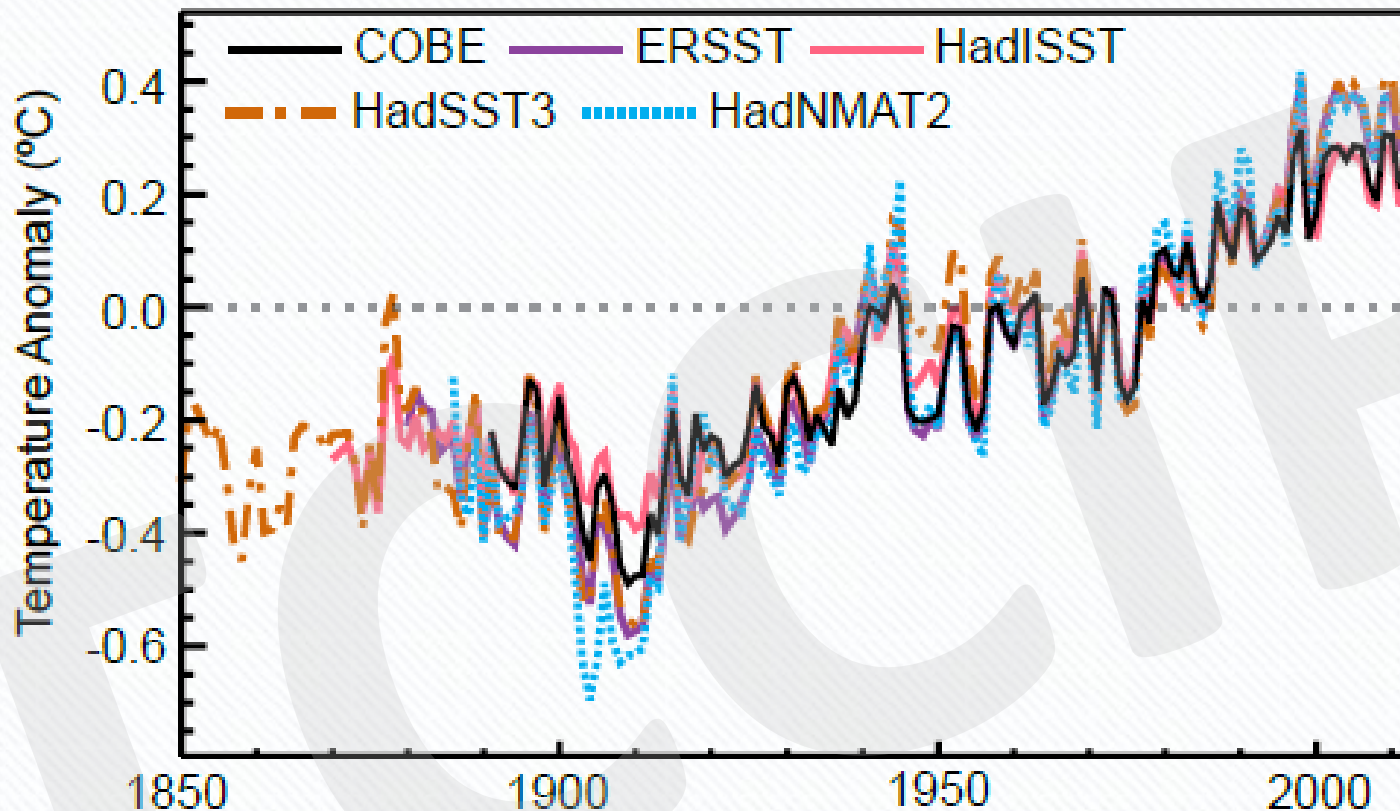


**Figure 2.18:** Global annual average Sea Surface Temperature (SST) and Night Marine Air Temperature (NMAT) relative to a 1961–1990 climatology from state of the art datasets. Spatially interpolated products are shown by solid lines; non-interpolated products by dashed lines.

# 全球地表溫度

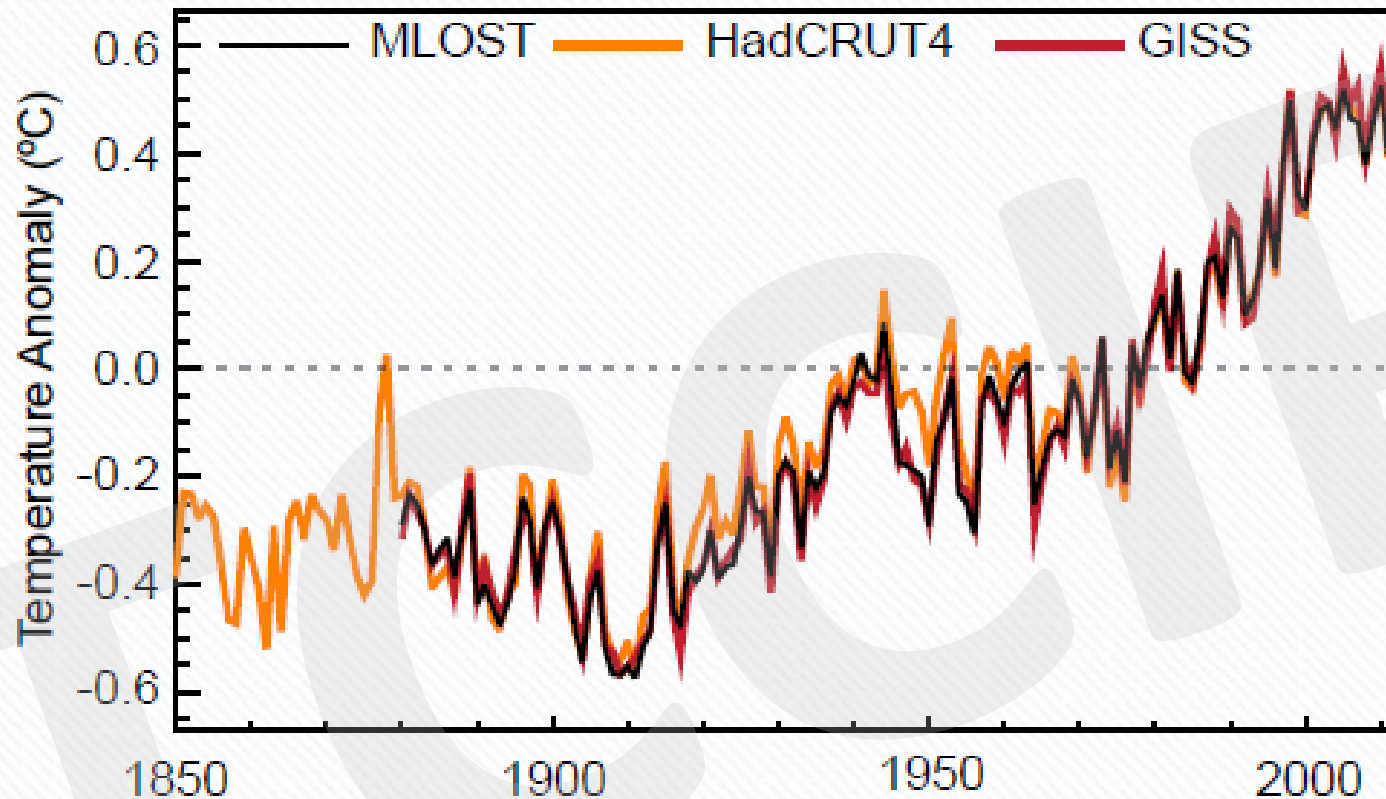


**Figure 2.20:** Annual Global Mean Surface Temperature (GMST) anomalies relative to a 1961–1990 climatology from the latest version of the three combined Land-Surface Air Temperature (LSAT) and Sea Surface Temperature (SST) datasets (HadCRUT4, GISS and NCDC MLOST). Published dataset uncertainties are not included for reasons discussed in Box 2.1.

✿ 除了明顯的多年代尺度的暖化，全球平均地表溫度也呈現明顯的年代和年際尺度變化。由於自然的變異，依據短期紀錄計算得的趨勢容易受起始和結束日期選擇的影響，通常無法反應長期的氣候趨勢。例如，因為起始年正好是一個強烈聖嬰事件，過去15年的暖化速率(1998–2012年；每十年0.05 [-0.05–0.15]°C)就小於從1951年開始計算的暖化速率(1951–2012年；每十年0.12 [0.08–0.14]°C)。



# 全球地表溫度的年代變化

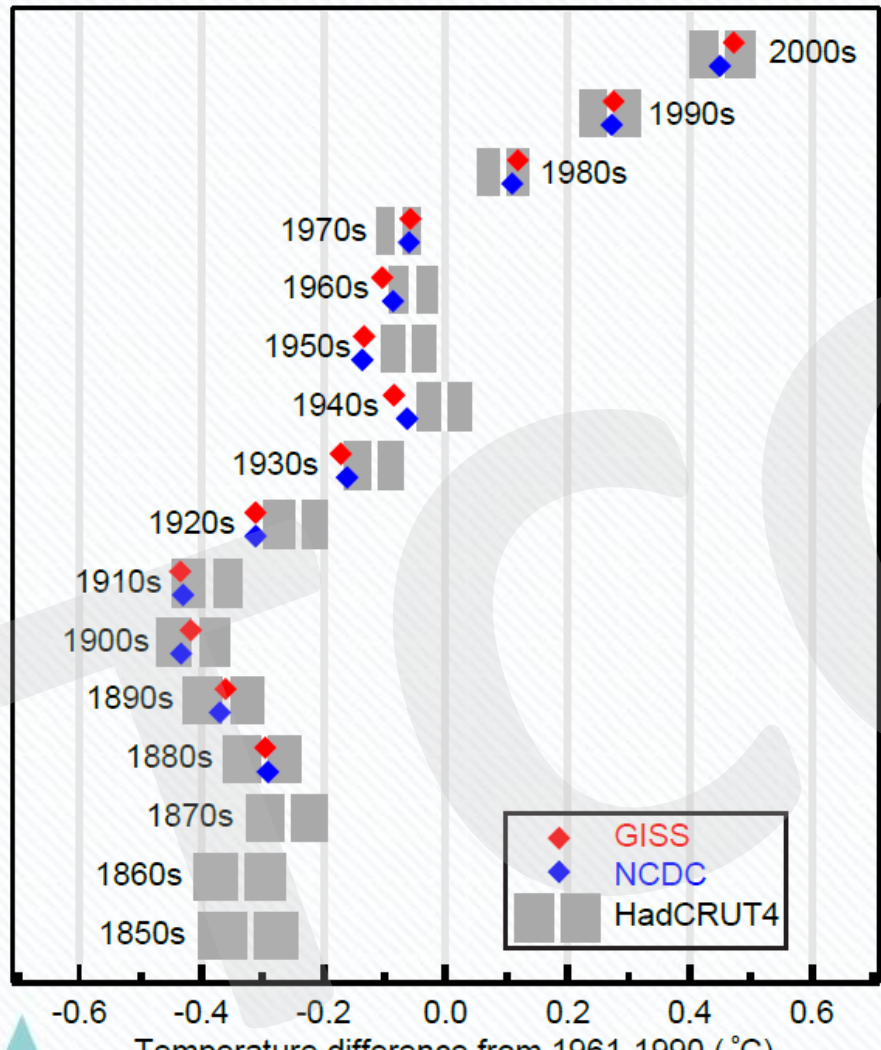
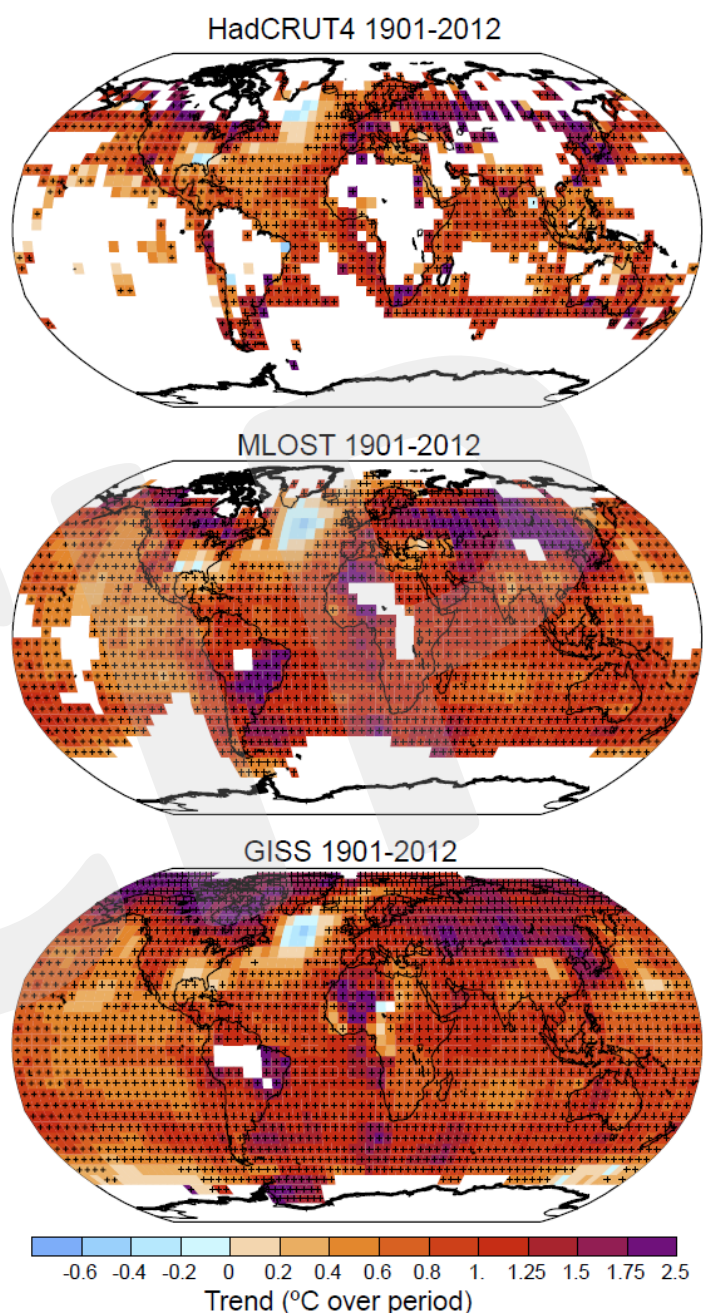


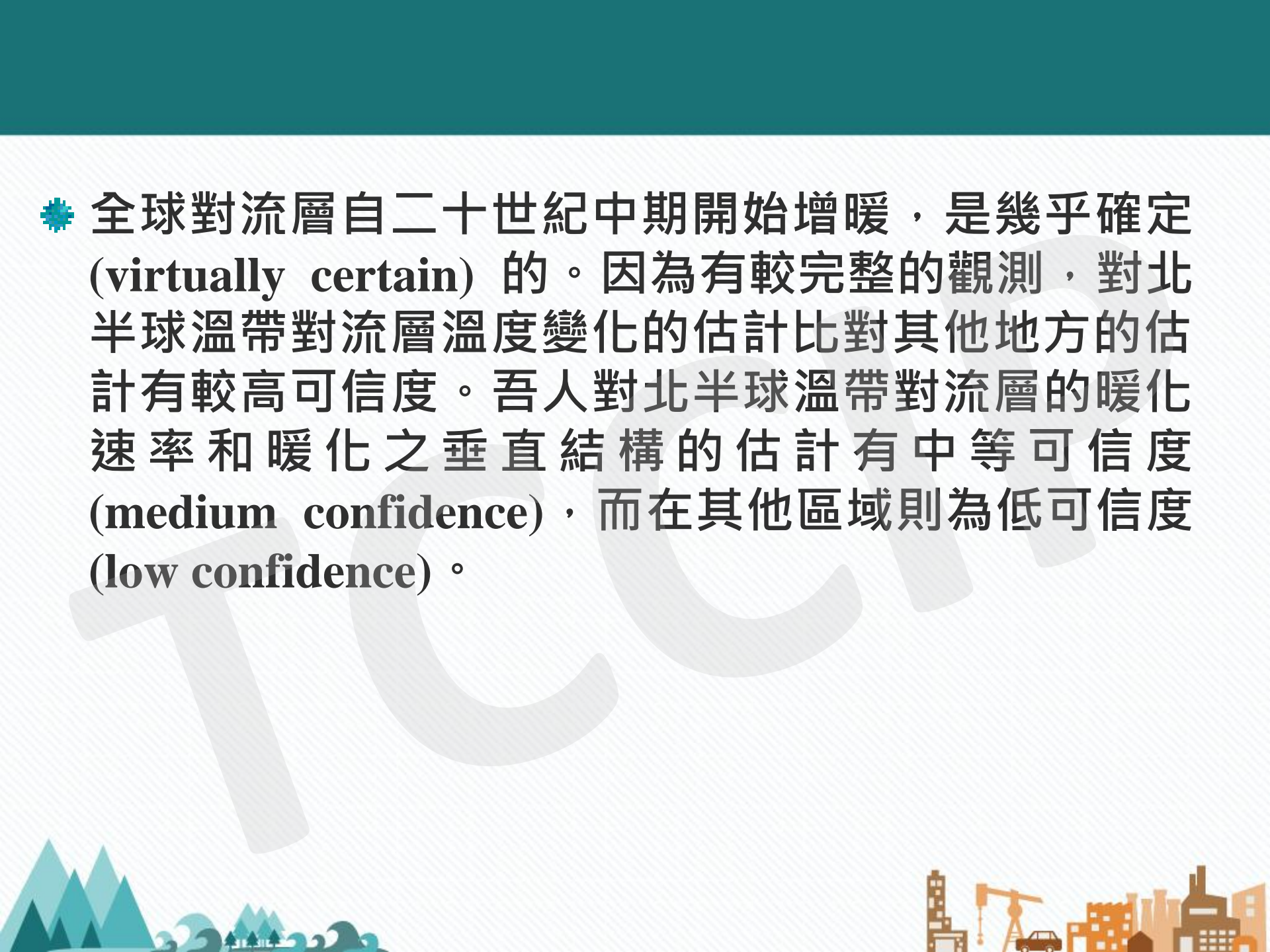
**Figure 2.19:** Decadal Global Mean Surface Temperature (GMST) anomalies (white vertical lines in grey blocks) and their uncertainties (90% confidence intervals as grey blocks) based upon the Land-Surface Air Temperature (LSAT) and Sea Surface Temperature (SST) combined HadCRUT4 (v4.1.1.0) ensemble (Morice et al., 2012). Anomalies are relative to a 1961–1990 climatology. 1850s indicates the period 1850–1859, and so on. NCDC MLOST and GISS dataset best-estimates are also shown.

# 地表溫度變率的分布

**Figure 2.21:** Trends in Global Mean Surface Temperature (GMST) from the three datasets of Figure 2.20 for 1901–2012. White areas indicate incomplete or missing data. Trends have been calculated only for those grid boxes with greater than 70% complete records and more than 20% data availability in first and last decile of the period. Black plus signs (+) indicate grid boxes where trends are significant (i.e., a trend of zero lies outside the 90% confidence interval). Differences in coverage primarily reflect the degree of interpolation to account for data void regions undertaken by the dataset providers ranging from none beyond grid box averaging (HadCRUT4) to substantial (GISS).



✿ 全球對流層自二十世紀中期開始增暖，是幾乎確定 (virtually certain) 的。因為有較完整的觀測，對北半球溫帶對流層溫度變化的估計比對其他地方的估計有較高可信度。吾人對北半球溫帶對流層的暖化速率和暖化之垂直結構的估計有中等可信度 (medium confidence)，而在其他區域則為低可信度 (low confidence)。



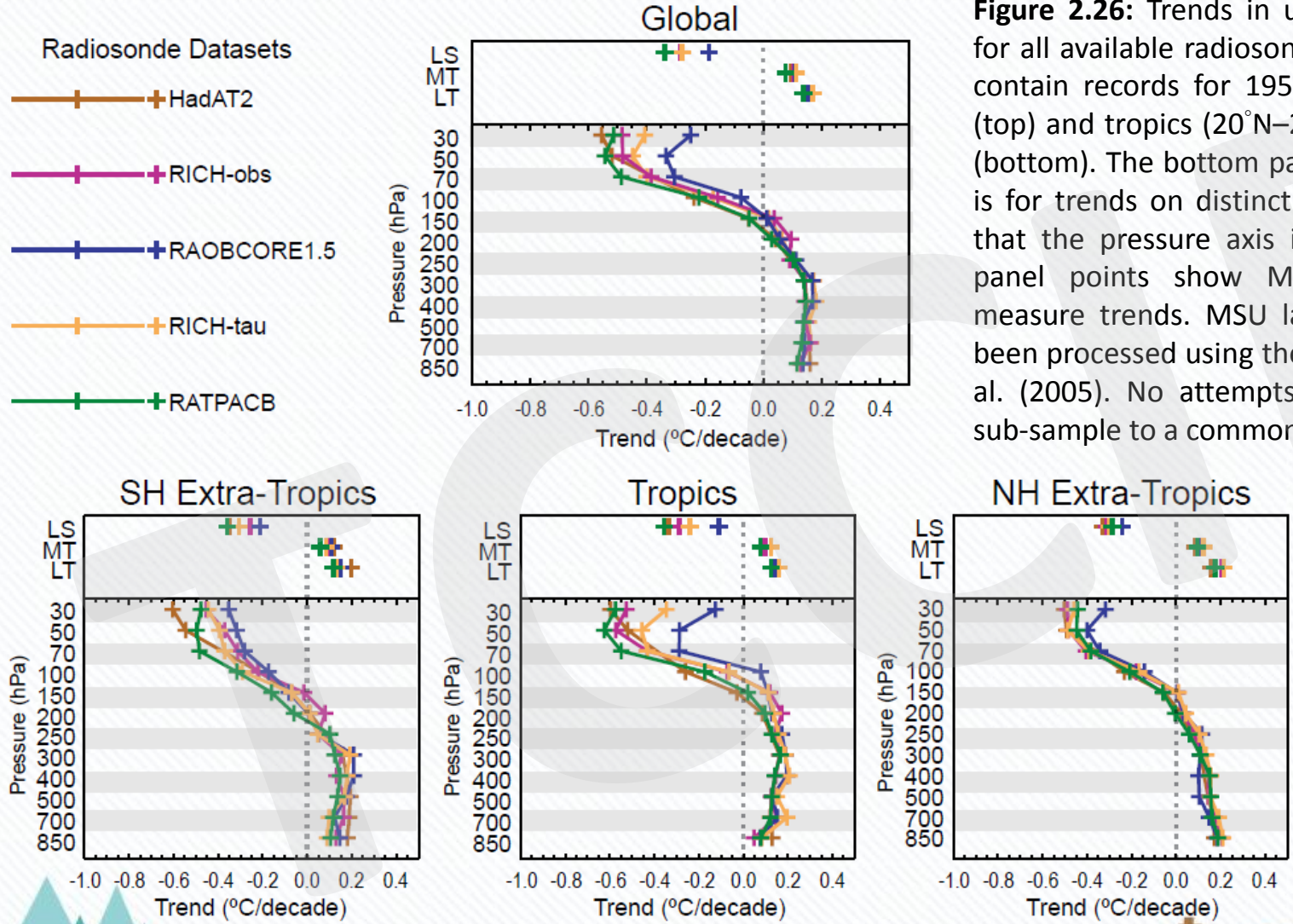


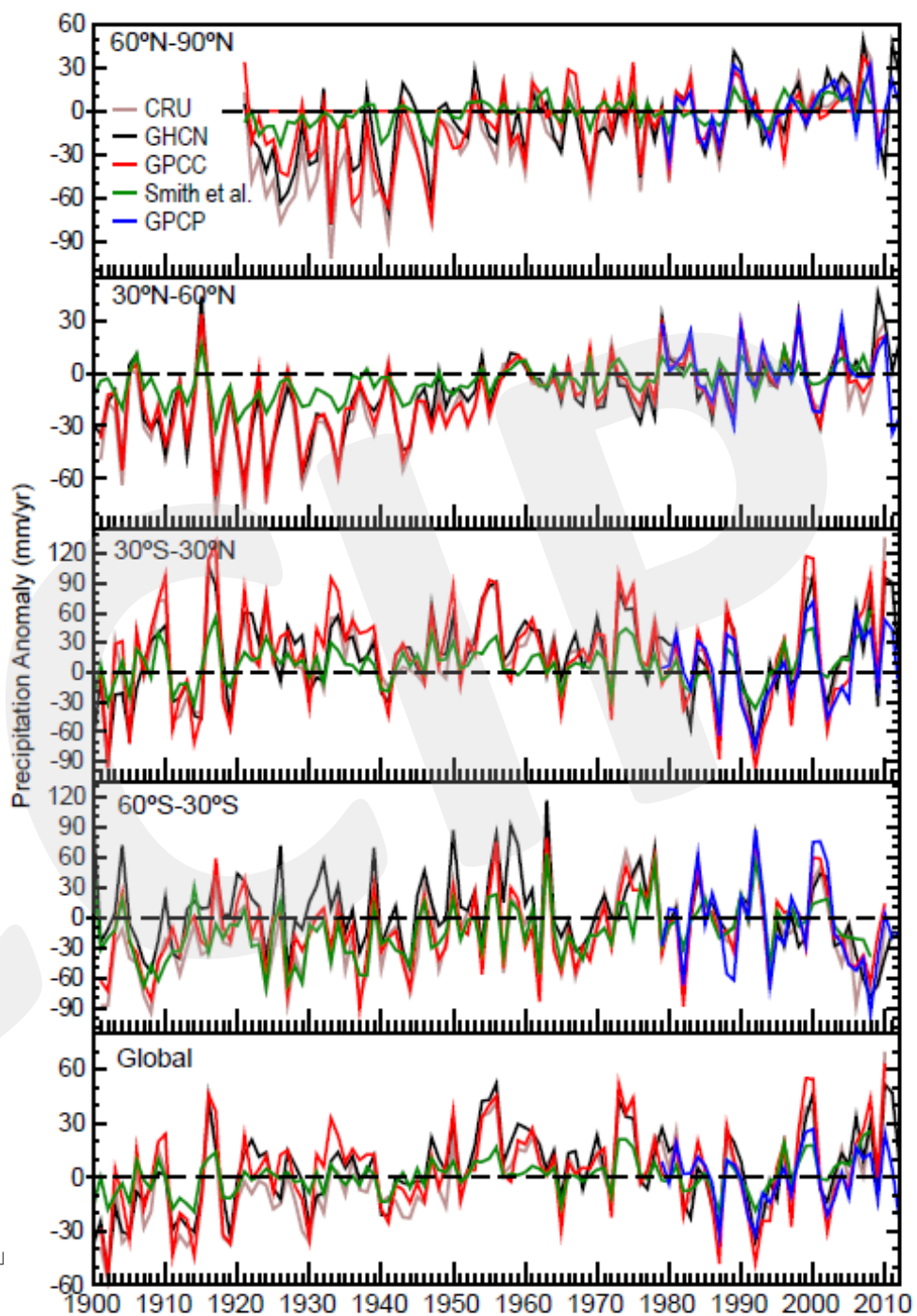
**Figure 2.26:** Trends in upper air temperature for all available radiosonde data products that contain records for 1958–2012 for the globe (top) and tropics ( $20^{\circ}\text{N}$ – $20^{\circ}\text{S}$ ) and extra-tropics (bottom). The bottom panel trace in each case is for trends on distinct pressure levels. Note that the pressure axis is not linear. The top panel points show MSU layer equivalent measure trends. MSU layer equivalents have been processed using the method of Thorne et al. (2005). No attempts have been made to sub-sample to a common data mask.

✿ 對於1901年以後全球陸地的平均降水量變化之估計，在1951年以前是低 (low) 可信度，而1951年之後則為中等 (medium) 可信度。自1901年起，北半球中緯度陸地平均的降水量是增加的 (1951年以前為中等可信度 medium confidence，而之後則為高可信度high confidence)。其他緯度地區的長期區域平均之正負趨勢皆呈現低可信度 (low confidence)。



# 全球降雨變化

**Figure 2.28:** Annual precipitation anomalies averaged over land areas for four latitudinal bands and the globe from five global precipitation datasets relative to a 1981–2000 climatology.



引用自「IPCC氣候變遷第五次評估報告」

# 降雨變化的分布

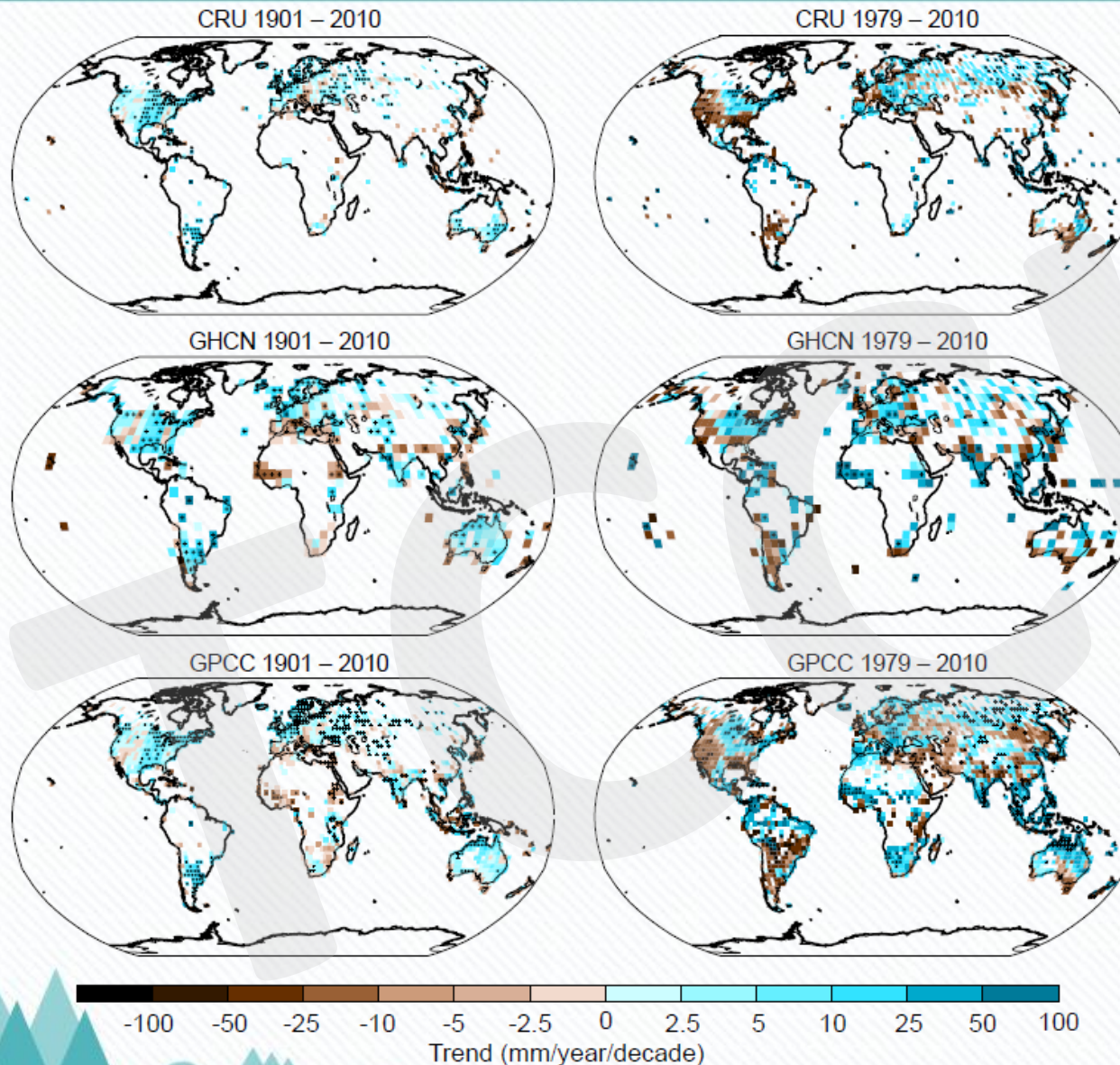


**Figure 2.29:** Trends in precipitation over land from the CRU, GHCN and GPCC datasets for 1901–2010 (left hand panels) and 1979–2010 (right hand panels). Trends have been calculated only for those grid boxes with greater than 70% complete records and more than 20% data availability in first and last decile of the period. White areas indicate incomplete or missing data. Black plus signs (+) indicate grid boxes where trends are significant (i.e., a trend of zero lies outside the 90% confidence interval).

# 近地面水氣的變化

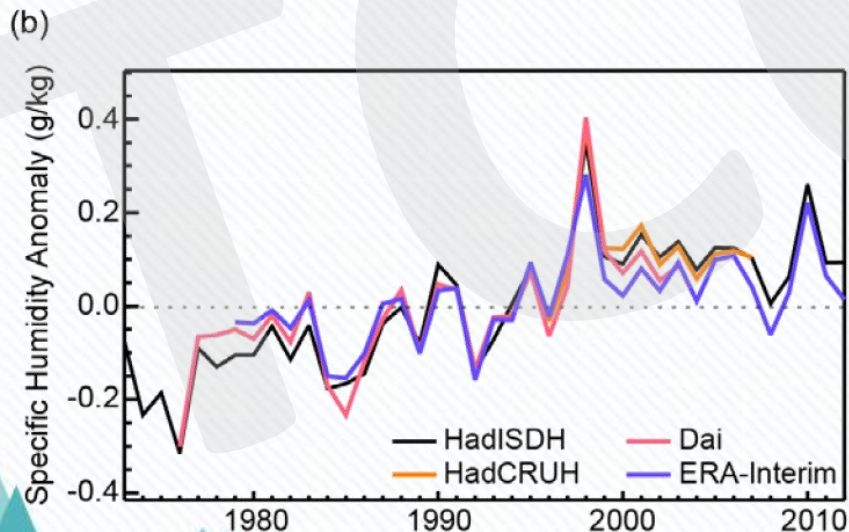
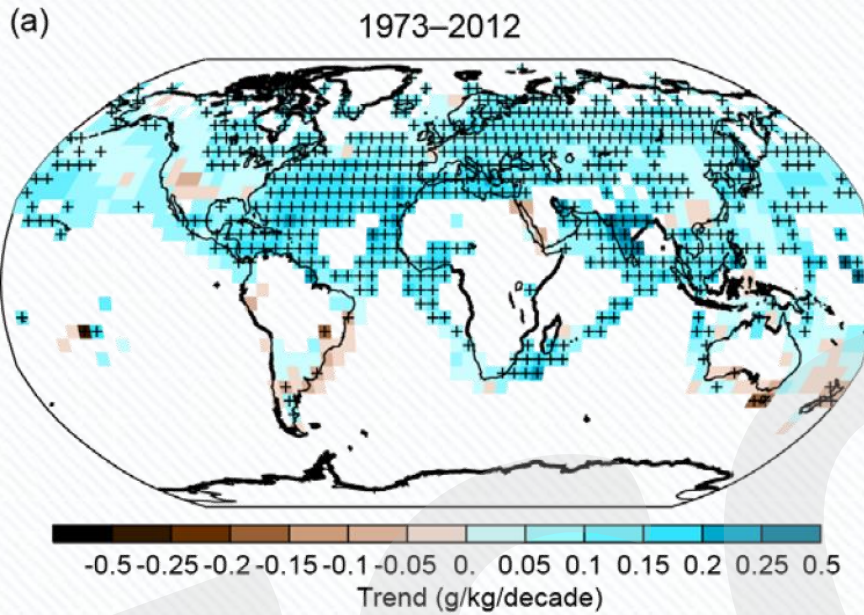


**Figure 2.30:** a) Trends in surface specific humidity from HadISDH and NOCS over 1973–2012. Trends have been calculated only for those grid boxes with greater than 70% complete records and more than 20% data availability in first and last decile of the period. White areas indicate incomplete or missing data. Black plus signs (+) indicate grid boxes where trends are significant (i.e., a trend of zero lies outside the 90% confidence interval). b) Global annual average anomalies in land surface specific humidity from Dai (2006; red), HadCRUH (Willett et al., 2013; orange), HadISDH (Willett et al., 2013; black), and ERA-Interim (Simmons et al., 2010; blue). Anomalies are relative to the 1979–2003 climatology.

# 大氣水氣含量的變化

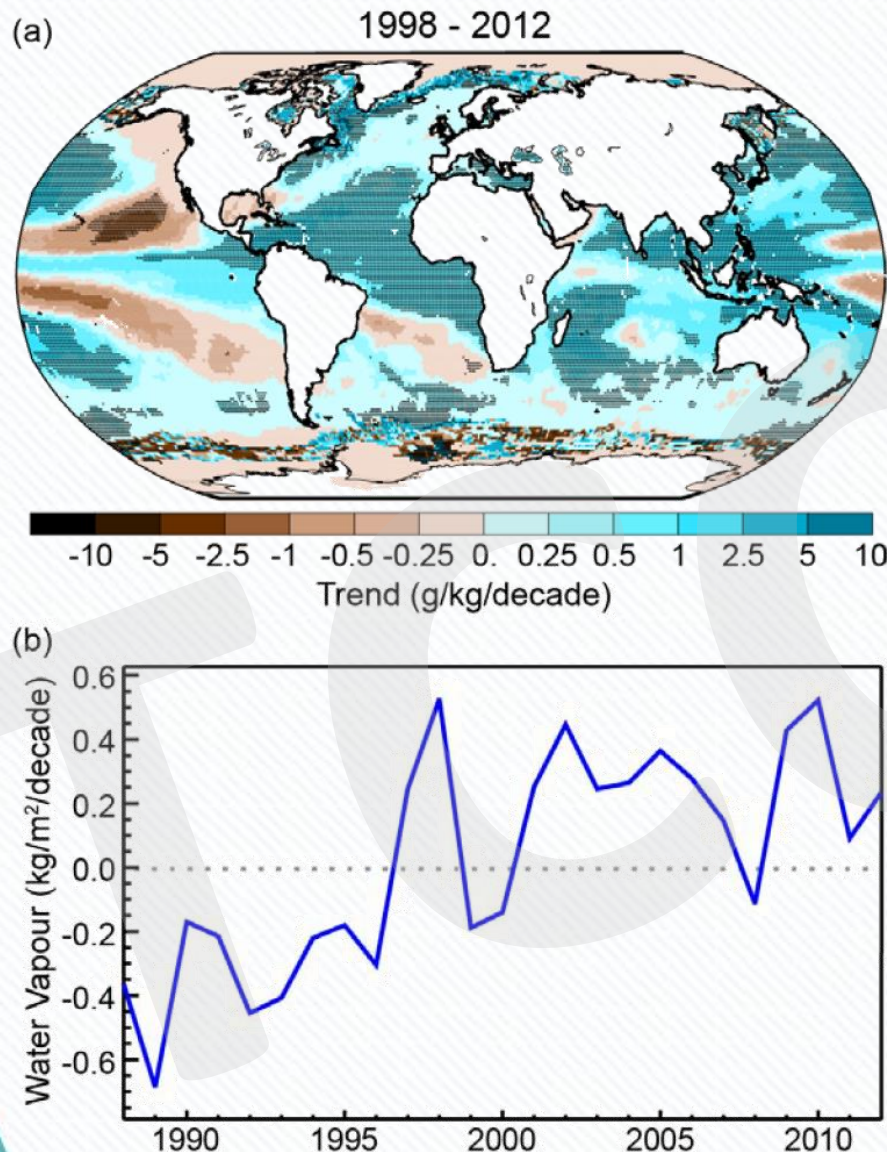
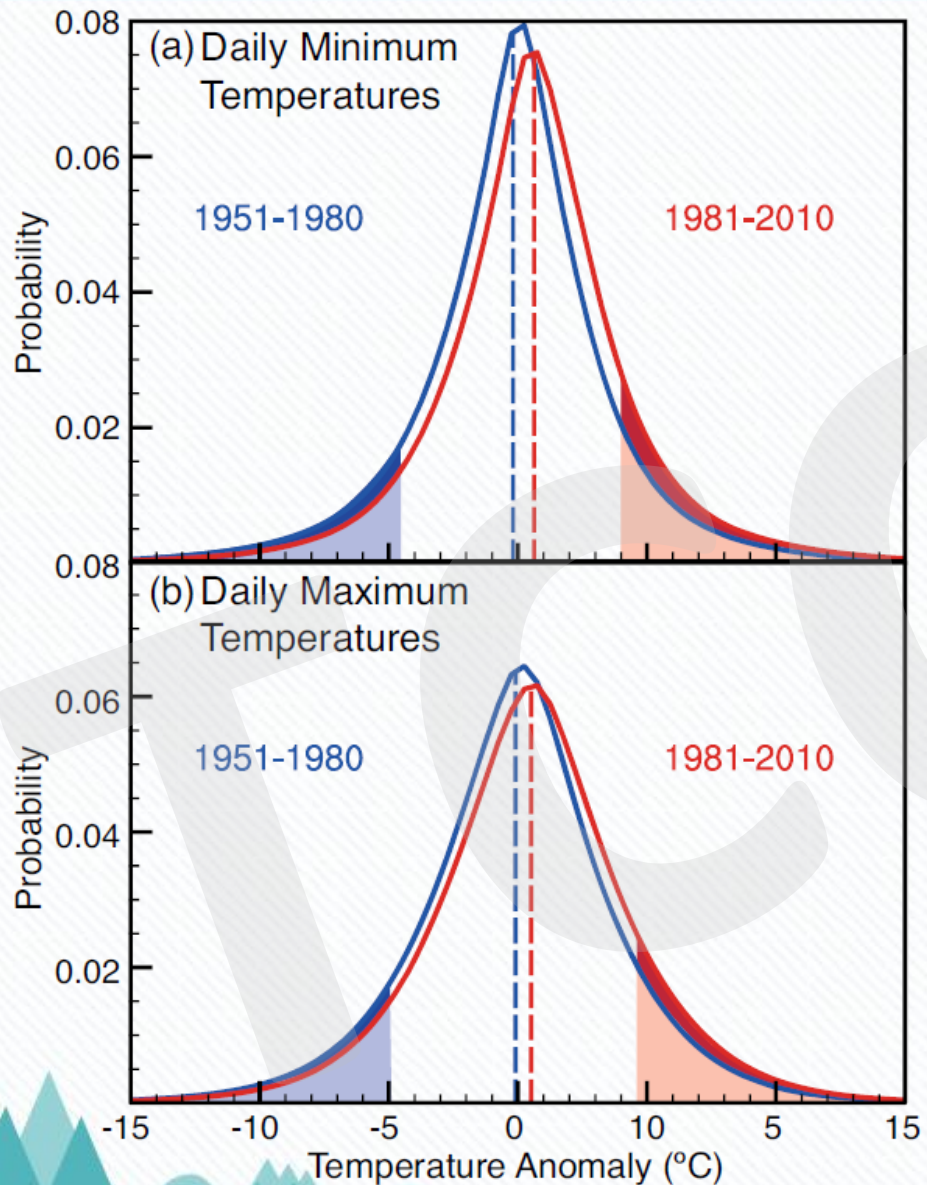


**Figure 2.31:** a) Trends in column integrated water vapour over ocean surfaces from Special Sensor Microwave Imager, (Wentz et al., 2007) for the period 1988–2010. Trends have been calculated only for those grid boxes with greater than 70% complete records and more than 20% data availability in first and last decile of the period. Black plus signs (+) indicate grid boxes where trends are significant (i.e., a trend of zero lies outside the 90% confidence interval). b) Global annual average anomalies in column integrated water vapour averaged over ocean surfaces. Anomalies are relative to the 1988–2007 average.

※ 約自1950年起，人類已觀測到許多極端天氣和氣候事件的變遷。非常可能 (very likely) 的是，全球的寒日和寒夜的次數已經減少，而熱日和熱夜的次數已經增加。在歐洲、亞洲、和澳洲的大範圍區域，熱浪的頻率可能 (likely) 已經增加。陸地上豪大雨事件增加的區域可能 (likely) 多於減少的區域。在北美和歐洲，豪大雨事件的頻率和強度可能 (likely) 已經增加。而對於其他陸塊上的豪大雨事件變化的評估最多只有中等可信度 (medium confidence)。



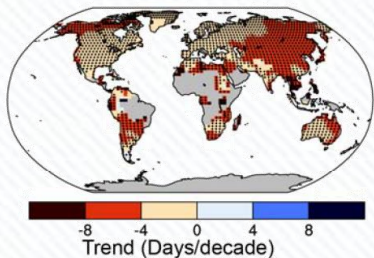
# 日最高溫和最低溫的變化分布



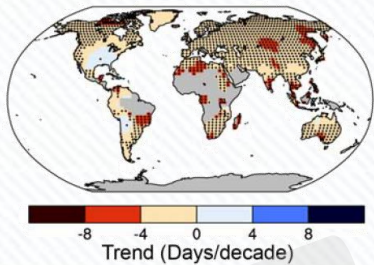
**FAQ 2.2, Figure 1:** Distribution of (a) daily minimum and (b) daily maximum temperature anomalies relative to a 1961–1990 climatology for two periods: 1951–1980 (blue) and 1981–2010 (red) using the HadGHCND dataset. The shaded blue and red areas represent the coldest 10% and warmest 10% respectively of (a) nights and (b) days during the 1951–1980 period. The darker shading indicates by how much the number of the coldest days and nights has reduced (dark blue) and by how much the number of the warmest days and nights has increased (dark red) during the 1981–2010 period compared to the 1951–1980 period.

# 極端溫度的變化分布

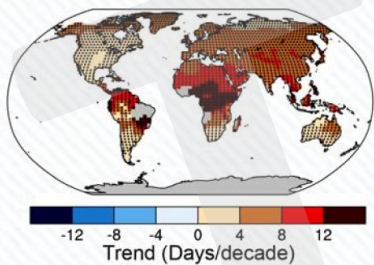
(a) Cold Nights



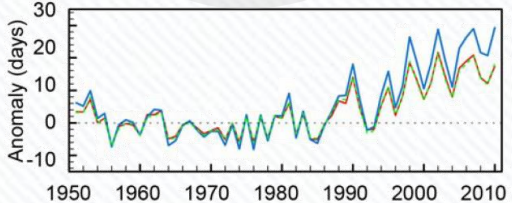
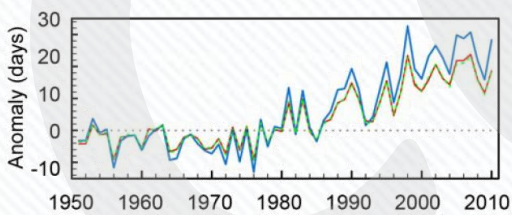
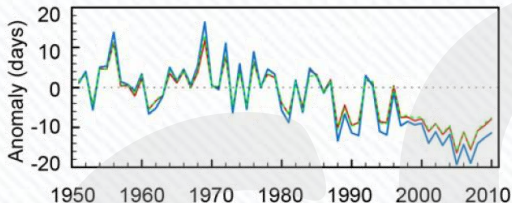
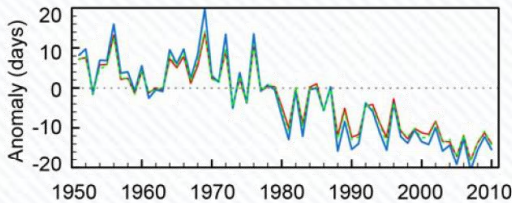
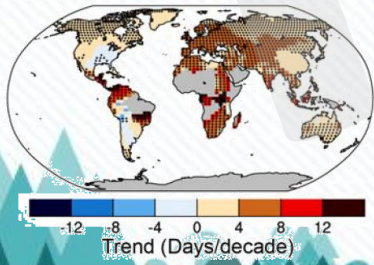
(b) Cold Days



(c) Warm Nights



(d) Warm Days

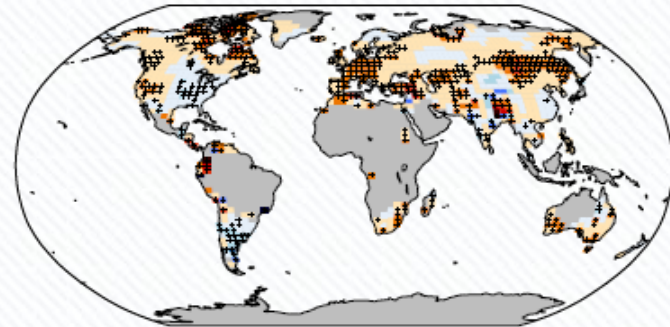


引用自「IPCC氣候變遷第五次評估報告」

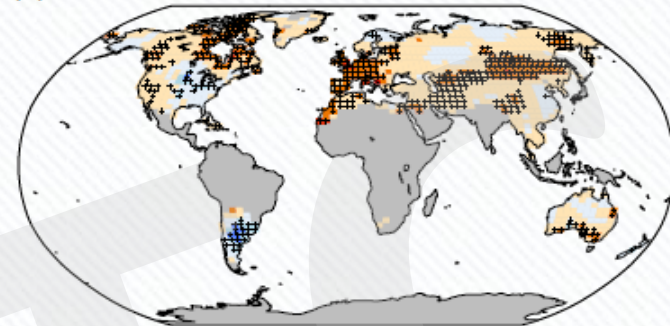
**Figure 2.32:** Trends in annual frequency of extreme temperatures over the period 1951–2010, for: (a) cold nights (TN10p), (b) cold days (TX10p), (c) warm nights (TN90p) and (d) warm days (TX90p) (Box 2.4, Table 1). Trends were calculated only for grid boxes that had at least 40 years of data during this period and where data ended no earlier than 2003. Grey areas indicate incomplete or missing data. Black plus signs (+) indicate grid boxes where trends are significant (i.e., a trend of zero lies outside the 90% confidence interval). The data source for trend maps is HadEX2 (Donat et al., 2013c) updated to include the latest version of the European Climate Assessment dataset (Klok and Tank, 2009). Beside each map are the near-global time series of annual anomalies of these indices with respect to 1961–1990 for three global indices datasets: HadEX2 (red); HadGHCND (Caesar et al., 2006; blue) and updated to 2010 and GHCNDEX (Donat et al., 2013a; green). Global averages are only calculated using grid boxes where all three datasets have at least 90% of data over the time period. Trends are significant (i.e., a trend of zero lies outside the 90% confidence interval) for all the global indices shown.

# 熱浪事件的變化分布

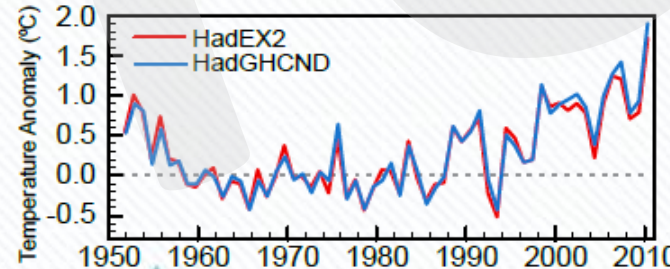
(a) HadEX2 1951-2010



(b) HadGHCND 1951-2010



(c) Global Land Average



**Box 2.4, Figure 1:** Trends in the warmest day of the year using different datasets for the period 1951–2010. The datasets are (a) HadEX2 (Donat et al., 2013c) updated to include the latest version of the European Climate Assessment dataset (Klok and Tank, 2009), (b) HadGHCND (Caesar et al., 2006) using data updated to 2010 (Donat et al., 2013a), and (c) Globally averaged annual warmest day anomalies for each dataset. Trends were calculated only for grid boxes that had at least 40 years of data during this period and where data ended no earlier than 2003. Grey areas indicate incomplete or missing data. Black plus signs (+) indicate grid boxes where trends are significant (i.e., a trend of zero lies outside the 90% confidence interval). Anomalies are only calculated using grid boxes where both datasets have data and where 90% of data are available.

# 極端降雨和乾旱的變化分布

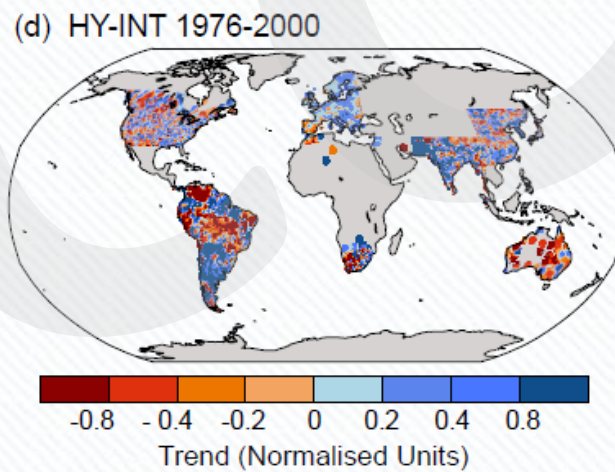
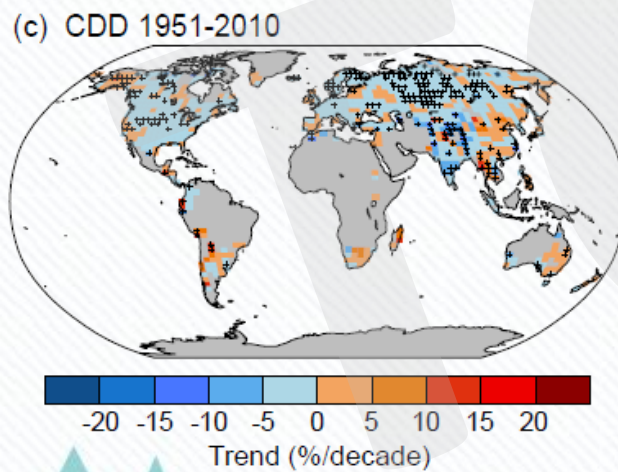
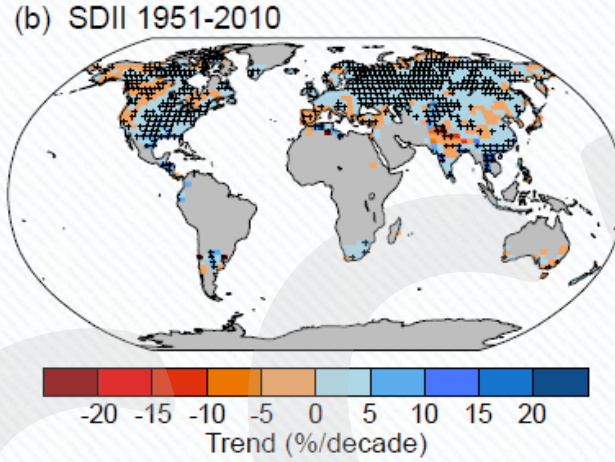
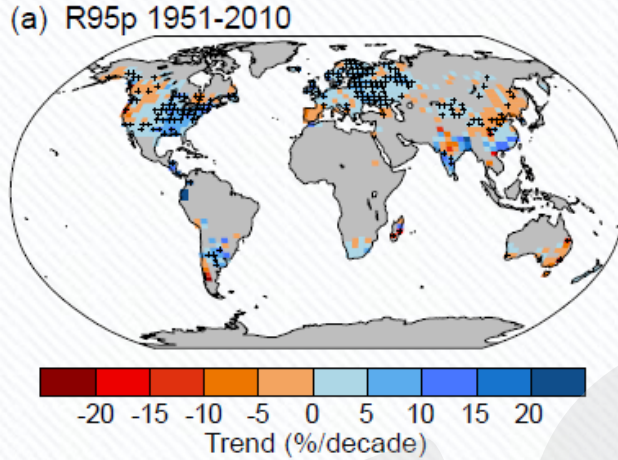


**Figure 2.33:** Trends in (a) annual amount of precipitation from days >95th percentile (R95p) (b) daily precipitation intensity (SDII) and (c) frequency of the annual maximum number of consecutive dry days (CDD) (Box 2.4, Table 1). Trends are shown as relative values for better comparison across different climatic regions. Trends were calculated only for grid boxes that had at least 40 years of data during this period and where data ended no earlier than 2003. Grey areas indicate incomplete or missing data. Black plus signs (+) indicate grid boxes where trends are significant (i.e., a trend of zero lies outside the 90% confidence interval). The data source for trend maps is HadEX2 (Donat et al., 2013a) updated to include the latest version of the European Climate Assessment dataset (Klok and Tank, 2009). (d) Trends (normalized units) in hydroclimatic intensity (HY-INT: a multiplicative measure of length of dry spell and precipitation intensity) over the period 1976–2000 (adapted from Giorgi et al. (2011)). An increase (decrease) in HY-INT reflects an increase (decrease) in the length of drought and /or extreme precipitation events.

# 登陸颱風的變化

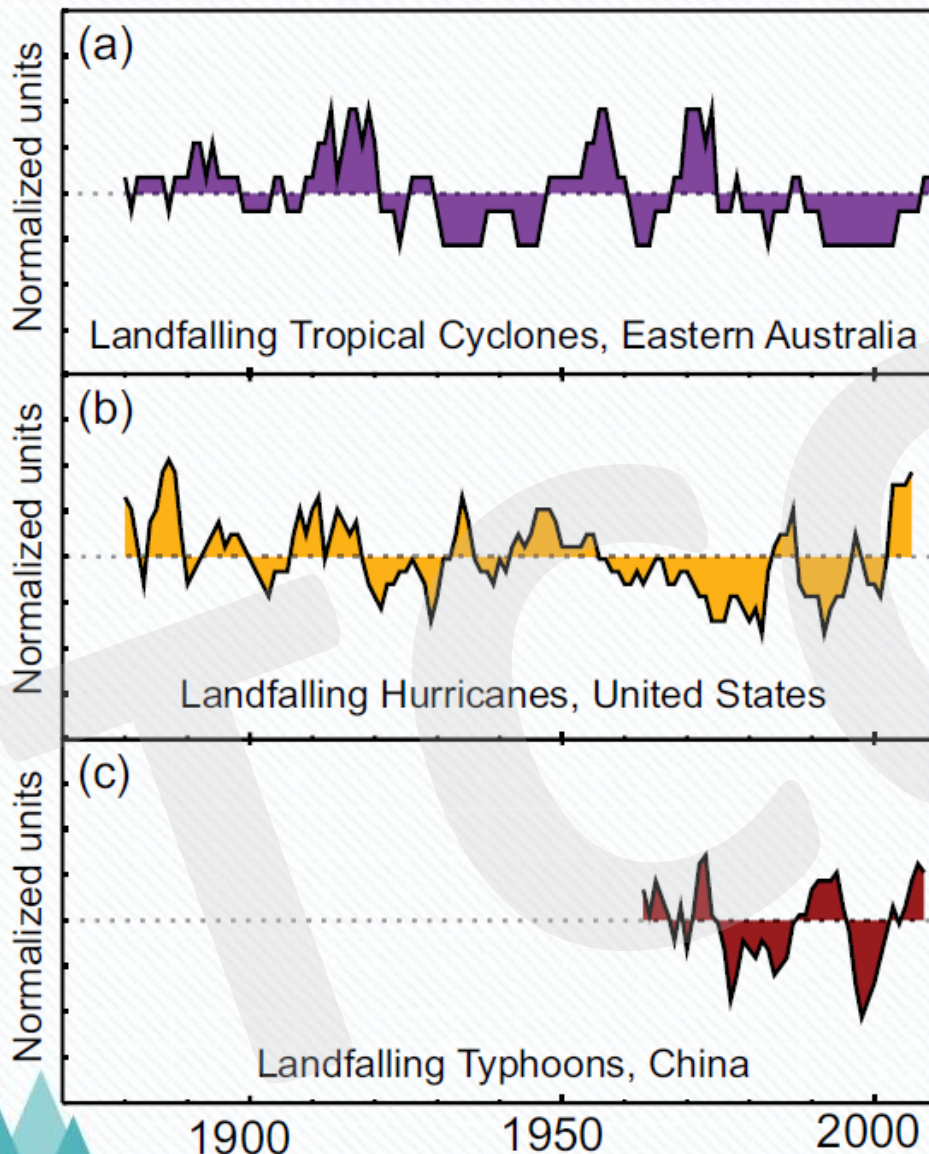


**Figure 2.34:** Normalized 5-year running means of the number of (a) adjusted land falling eastern Australian tropical cyclones (adapted from Callaghan and Power (2011) and updated to include 2010/2011 season) and (b) unadjusted land falling U.S. hurricanes (adapted from Vecchi and Knutson (2011)) and (c) land-falling typhoons in China (adapted from CMA, 2011). Vertical axis ticks represent one standard deviation, with all series normalized to unit standard deviation after a 5-year running mean was applied.

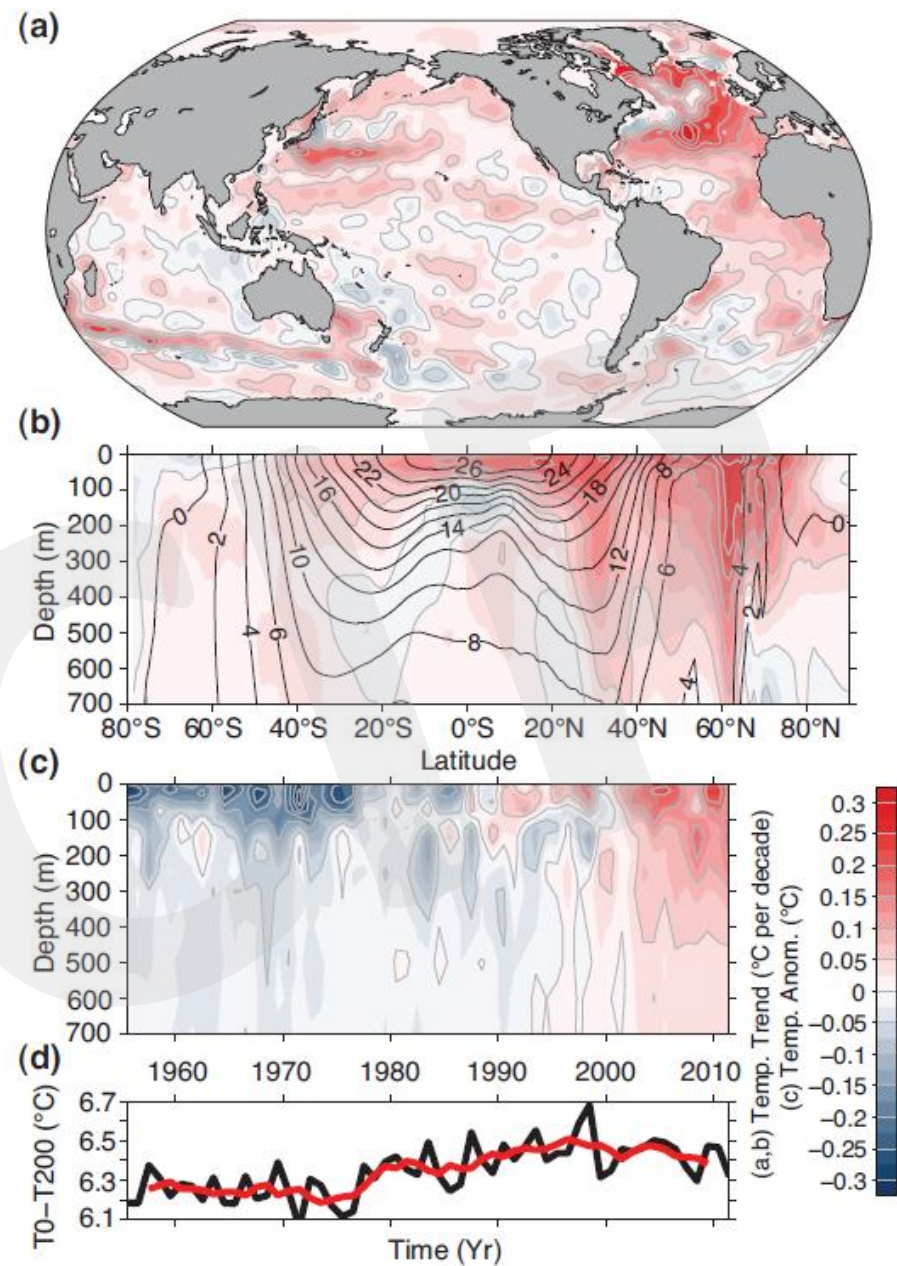
- ✿ 就全球尺度而言，海洋暖化最多的是在接近海表面之處。在1971-到2010年間，海平面以下75公尺以內的上層海水每十年增暖 $0.11[0.09-0.13]^\circ\text{C}$ 。自AR4發表後，吾人已辨識出上層海水溫度紀錄的儀器偏差並且已經減少了這些偏差，因此對這些變遷的評估更具信心。
- ✿ 自1957至2009年間，海平面以下700-2000公尺間的海水可能 (likely) 增暖了。自1992年至2005年間，已有足夠的觀測可提供科學家評估全球海平面2000公尺以下的溫度變化。這段時間內，海平面以下2000公尺至3000公尺之間的觀測海溫可能 (likely) 沒有顯著的變化趨勢，海平面以下3000公尺到海底之間的海水可能 (likely) 增暖，增暖最多的是南大洋。

- ✿ 在具有相對較多觀測資料的1971-2010年四十年期間，氣候系統的淨能量增加量有超過60%是儲存在海洋上層 (0-700公尺)，約30%是儲存在海面700公尺以下。以線性趨勢估計，在這段期間上層海洋熱容量的增加可能 (likely) 為 $17 [15-19] \times 10^{22}\text{J}$ 。
- ✿ 在2003年至2010年間0-700公尺的海洋熱容量或許可能 (about as likely as not) 比1993-2002年增加得慢。在年際變化較小的700-2000公尺間海域，海洋對熱的吸收在1993-2009年間可能 (likely) 持續不減。

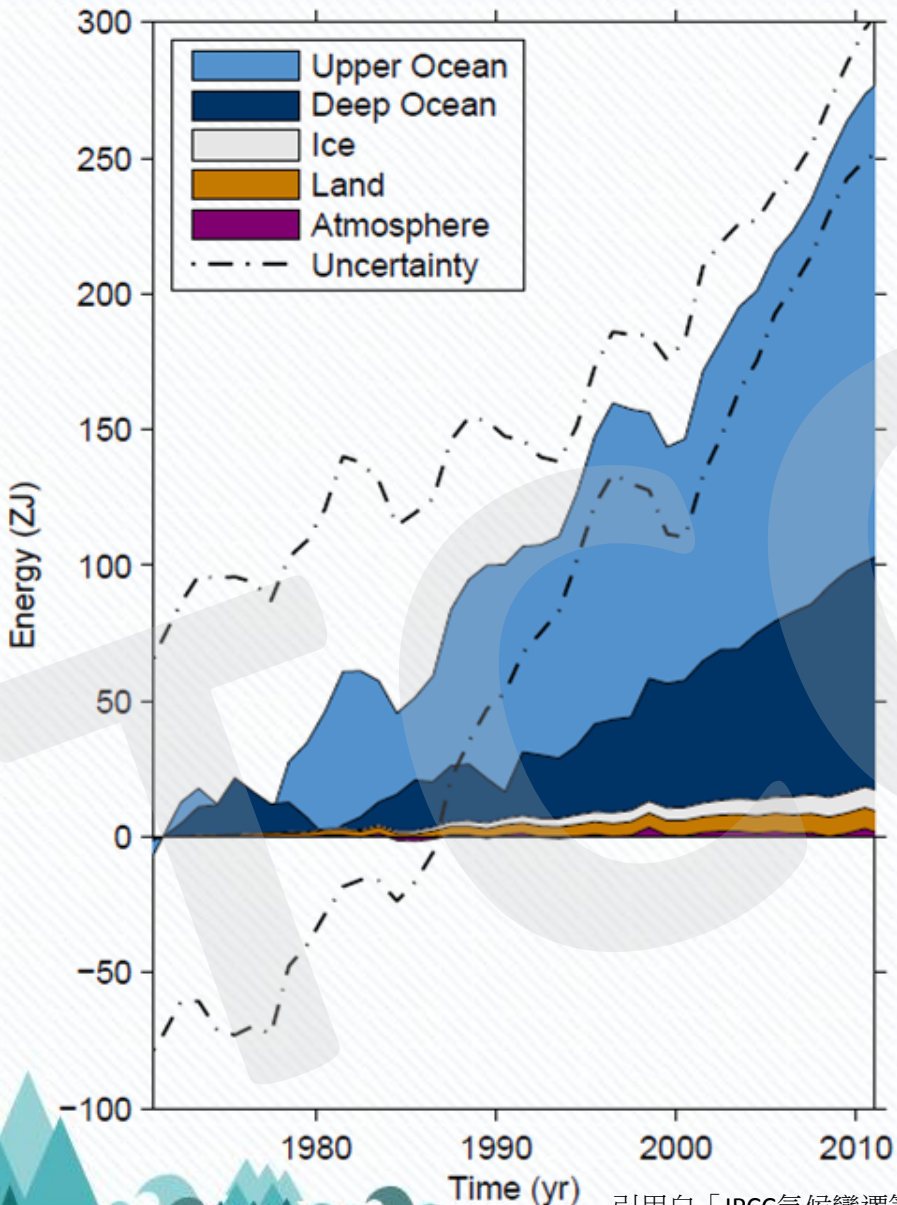
# 海水溫度的變化

Figure 3.1:

- a) Depth-averaged 0–700 m temperature trend for 1971–2010 (longitude vs. latitude, colors and grey contours in C per decade).
- b) Zonally-averaged temperature trends (latitude versus depth, colors and grey contours in C per decade) for 1971–2010, with zonally averaged mean temperature over-plotted (black contours in °C).
- c) Globally-averaged temperature anomaly (time versus depth, colors and grey contours in C) relative to the 1971–2010 mean.
- d) Globally-averaged temperature difference between the ocean surface and 200 m depth (black: annual values, red: 5-year running mean). All panels are constructed from an update of the annual analysis of Levitus et al. (2009).



# 海洋中熱含量的變化



**Box 3.1, Figure 1:** Plot of energy accumulation in ZJ ( $1 \text{ ZJ} = 1021 \text{ J}$ ) within distinct components of Earth's climate system relative to 1971 and from 1971–2010 unless otherwise indicated. See text for data sources. Ocean warming (heat content change) dominates, with the upper ocean (light blue, above 700 m) contributing more than the deep ocean (dark blue, below 700 m; including below 2000 m estimates starting from 1992). Ice melt (light grey; for glaciers and ice caps, Greenland and Antarctic ice sheet estimates starting from 1992, and Arctic sea ice estimate from 1979–2008); continental (land) warming (orange); and atmospheric warming (purple; estimate starting from 1979) make smaller contributions. Uncertainty in the ocean estimate also dominates the total uncertainty (dot-dashed lines about the error from all five components at 90% confidence intervals).

- ✿ 自1950年代以來，非常可能 (very likely) 在以蒸發為主的高鹽度海域中，海水已經變得更鹹，而在以降水為主的低鹽度海域，海水已經變得更淡。這種海水鹽度的區域變化趨勢間接證明海面的蒸發和降水已經改變 (中等可信度medium confidence)。

# 海表面能量和水氣交換的變化

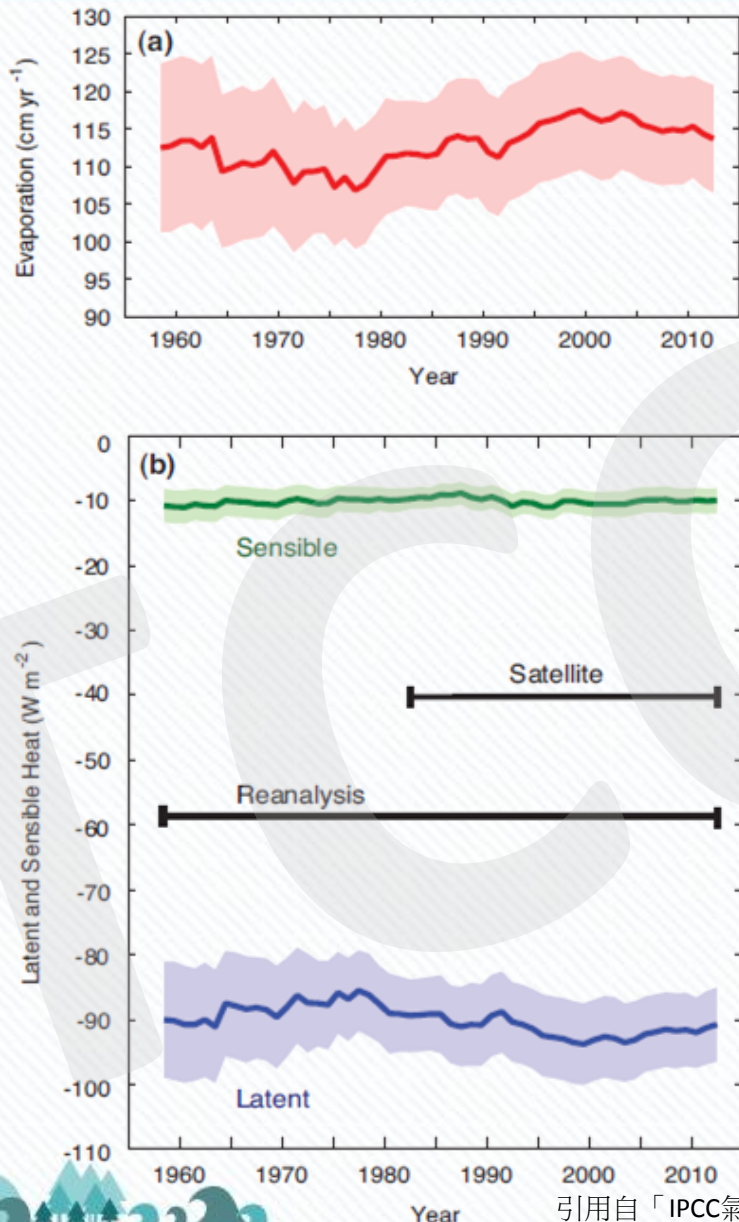
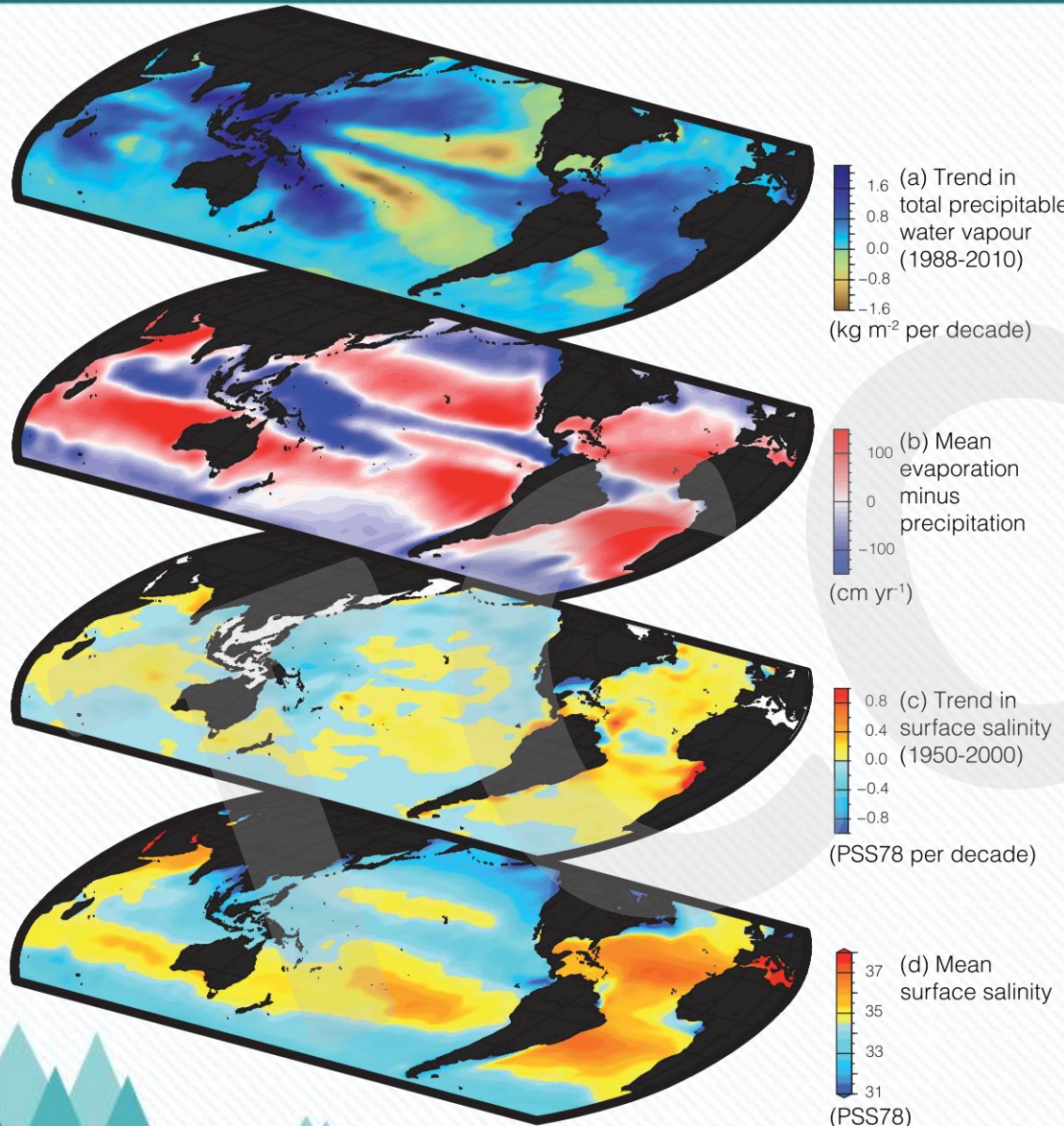


**Figure 3.6:** Time series of annual mean global ocean average evaporation (red line panel a), sensible heat flux (green line panel b) and latent heat flux (blue line panel b) from 1958 to 2012 determined by Yu from a revised and updated version of the original OAFlux dataset Yu and Weller (2007). Shaded bands show uncertainty estimates and the black horizontal bars in panel (b) show the time periods for which reanalysis output and satellite observations were employed in the OAFlux analysis; they apply to both panels.

# 海洋的氣候變遷



**FAQ 3.3, Figure 1:** Changes in sea surface salinity are related to the atmospheric patterns of Evaporation minus Precipitation (E-P) and trends in total precipitable water: a) Linear trend (1988–2010) in total precipitable water (water vapor integrated from Earth's surface up through the entire atmosphere) ( $\text{kg m}^{-2}$  per decade) from satellite observations (Special Sensor Microwave Imager) (after Wentz et al., 2007) (blues wetter; yellows drier). b) The 1979–2005 climatological mean net E-P ( $\text{cm yr}^{-1}$ ) from meteorological reanalysis (National Centers for Environmental Prediction/National Center for Atmospheric Research; Kalnay et al., 1996) (reds: net evaporation; blues: net precipitation). c) Trend (1950–2000) in surface salinity (PSS78 per 50 years) (after Durack and Wijffels, 2010) (blues freshening; yellows-reds saltier). d) The climatological-mean surface salinity (PSS78) (blues <35; yellows-reds >35).

- ✿ 代理數據 (proxy data) 和儀器監測數據顯示，十九世紀末期到二十世紀初期是海平面上升的轉變期，海平面上升速率從過去2000年以來相對較慢的速率轉變為較快 (高可信度high confidence)。可能 (likely) 自二十世紀初以來，全球海平面的平均上升速率就已經持續增加。
- ✿ 在1901年至2010年間，全球海平面的平均上升速率非常可能達 $1.7[1.5-1.9] \text{ mm yr}^{-1}$ ，在1971至2010年間非常可能為 $2.0[1.7-2.3] \text{ mm yr}^{-1}$ ，在1993年至2010年間非常可能已達 $3.2 [2.8-3.6] \text{ mm yr}^{-1}$ 。關於上述最後一個時期的較高上升速率，驗潮儀和衛星測高數據的結果是一致的。在1920年至1950年間也可能出現過類似的高海平面上升速率。

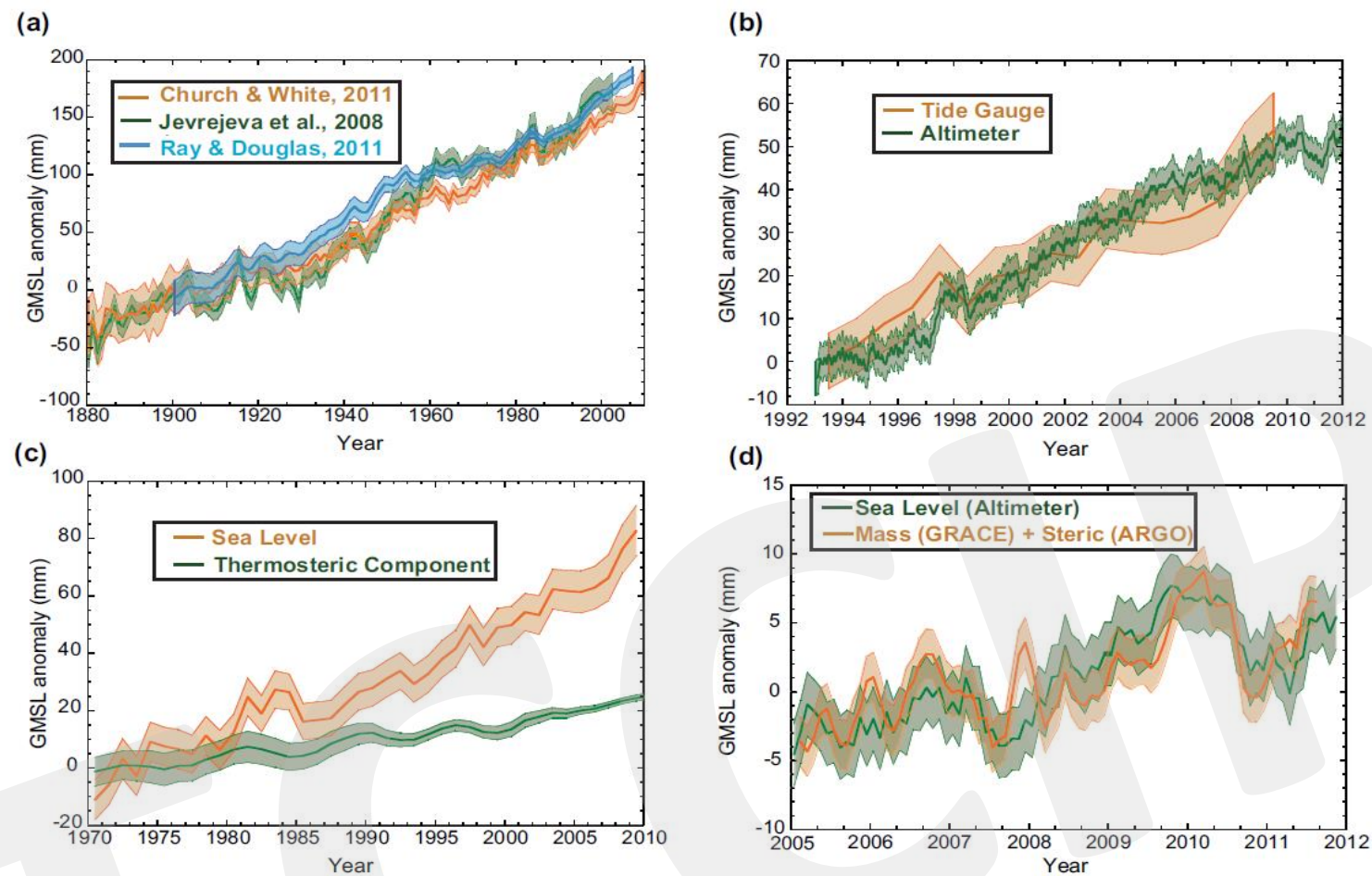
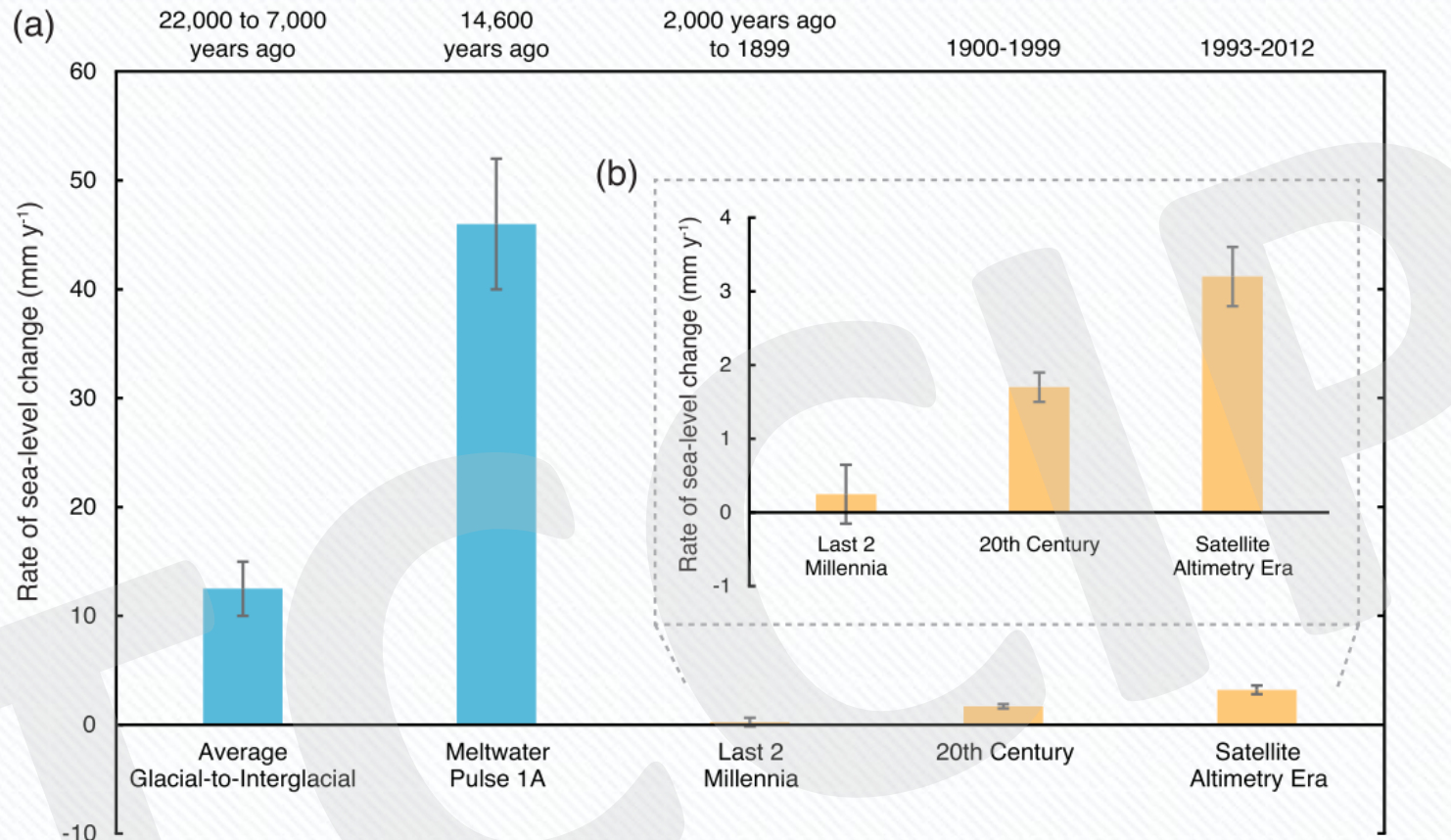


**Figure 3.13:** Global mean sea level anomalies (in mm) from the different measuring systems as they have evolved in time, plotted relative to 5-year mean values that start at **a)** 1900, **b)** 1993, **c)** 1970, and **d)** 2005. **a)** Yearly average GMSL reconstructed from tide gauges (1900–2010) by three different approaches (Jevrejeva et al., 2008; Church and White, 2011; Ray and Douglas, 2011), **b)** GMSL (1993–2010) from tide gauges and altimetry (Nerem et al., 2010) with seasonal variations removed and smoothed with a 60-day running mean **c)** GMSL (1970–2010) from tide gauges along with the thermosteric component to 700 m, (3-year running mean) estimated from in situ temperature profiles (updated from Domingues et al., 2008), **d)** the GMSL (nonsessional) from altimetry and that computed from the mass component (GRACE) and steric component (Argo) from 2005–2010 (Leuliette and Willis, 2011), all with a 3-month running mean filter. All uncertainty bars are one standard error as reported by the authors. The thermosteric component is just a portion of total sea level, and is not expected to agree with total sea level. 引用自「IPCC氣候變遷第五次評估報告」

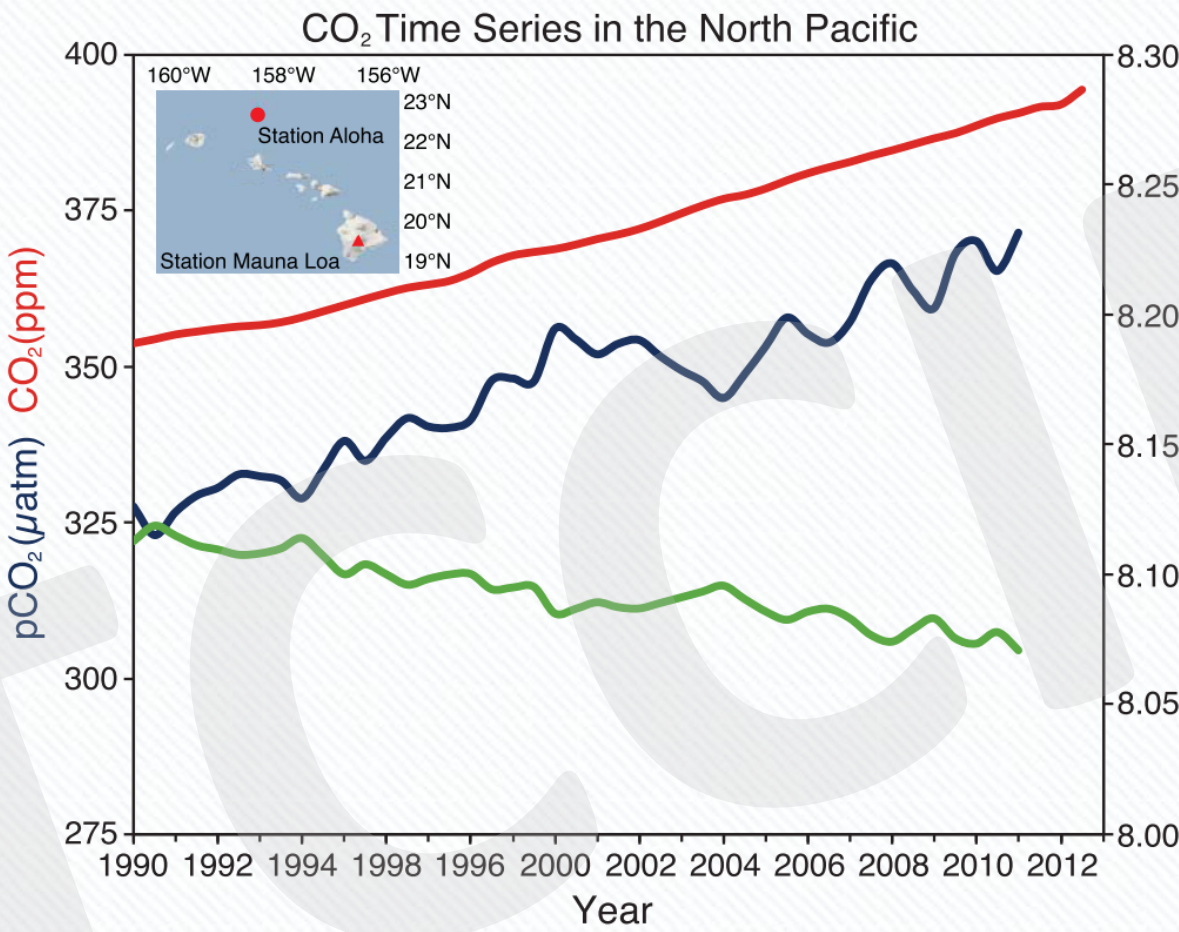
- \* 在上一次間冰期（距今129,000-116,000年）的數千年間，全球平均海平面的極大值至少比目前的海平面高出5公尺（非常高可信度 very high confidence）但不超過10公尺（高可信度 high confidence）。在上一次間冰期，格陵蘭冰層的變化非常可能導致全球平均海平面上升1.4-4.3公尺，這意味著海平面上升應該還有來自南極冰層融化的額外貢獻（中等可信度 medium confidence）。這些海平面的變遷，是在天文軌道作用力和現今不同且高緯地表溫度（就數千年平均而言）比現今至少高 $2^{\circ}\text{C}$ 的環境中發生（高可信度 high confidence）。



# 海平面變率的比較



**FAQ 5.2, Figure 1:** (a) Estimates of the average rate of global mean sea level change (in mm yr<sup>-1</sup>) for five selected time intervals: last glacial-to-interglacial transition; Meltwater Pulse 1a; last 2 millennia; 20th century; satellite altimetry era (1993–2012). Blue columns denote time intervals of transition from a glacial to an interglacial period, whereas orange columns denote the current interglacial period. Black bars indicate the range of likely values of the average rate of global mean sea level change. Note the overall higher rates of global mean sea level change characteristic of times of transition between glacial and interglacial periods. (b) Expanded view of the rate of global mean sea level change during three time intervals of the present interglacial.



**FAQ 3.2, Figure 1:** A smoothed time series of atmospheric CO<sub>2</sub> mole fraction (in ppm) at the atmospheric Mauna Loa Observatory (top red line), surface ocean partial pressure of CO<sub>2</sub> (pCO<sub>2</sub>; middle blue line), and surface ocean pH (bottom green line) at Station ALOHA in the subtropical North Pacific north of Hawaii for the period from 1990–2011 (after Doney et al., 2009; data from Dore et al., 2009). The results indicate that the surface ocean pCO<sub>2</sub> trend is generally consistent with the atmospheric increase but is more variable due to large-scale interannual variability of oceanic processes.

- ✿ 2002至2011年間，格陵蘭冰層的冰量損失平均速率非常可能 (very likely) 從1992至2001年間的34 [-6-74] Gt yr<sup>-1</sup>大幅增加為215 [157-274] Gt yr<sup>-1</sup>。{4.4}
- ✿ 南極冰層的冰量損失平均速率可能 (likely) 已經從1992至2001年間的30 [-37-97] Gt yr<sup>-1</sup>增加至2002-2011年間的147 [72-221] Gt yr<sup>-1</sup>。有非常高可信度顯示，這些損失主要來自北南極半島和西南極洲的阿蒙森海區域。

- ✿ 在1979至2012年間，北極海冰覆蓋範圍的年平均量持續減少，其速率非常可能 (very likely) 為每十年3.5%到4.1%之間 (即每十年0.45至0.51百萬平方公里)，而夏季海冰極低值 (常年海冰) 的減少速率非常可能 (very likely) 在每十年9.4%到13.6% (即每年0.73-1.07百萬平方公里) 之間。十年平均之北極海冰範圍的平均減少速率在夏季時最快 (高可信度high confidence)；自1979年以來，於每個連續的年代中，所有季節的海冰範圍都在減少 (高可信度high confidence)。根據資料重建結果，在過去三十年間，北極夏季海冰的縮減是史無前例的，而且過去至少1,450年以來海表面溫度異常地偏高 (中等可信度medium confidence)。
- ✿ 在1979至2012年間，南極海冰範圍的年平均量非常可能 (very likely) 以每十年1.2%至1.8%的速率增加 (即每十年0.13-0.20百萬平方公里)。有很高的可信度顯示，此年增加率有很大的區域差異，即在某些區域海冰範圍增加、而在其他區域則減少。

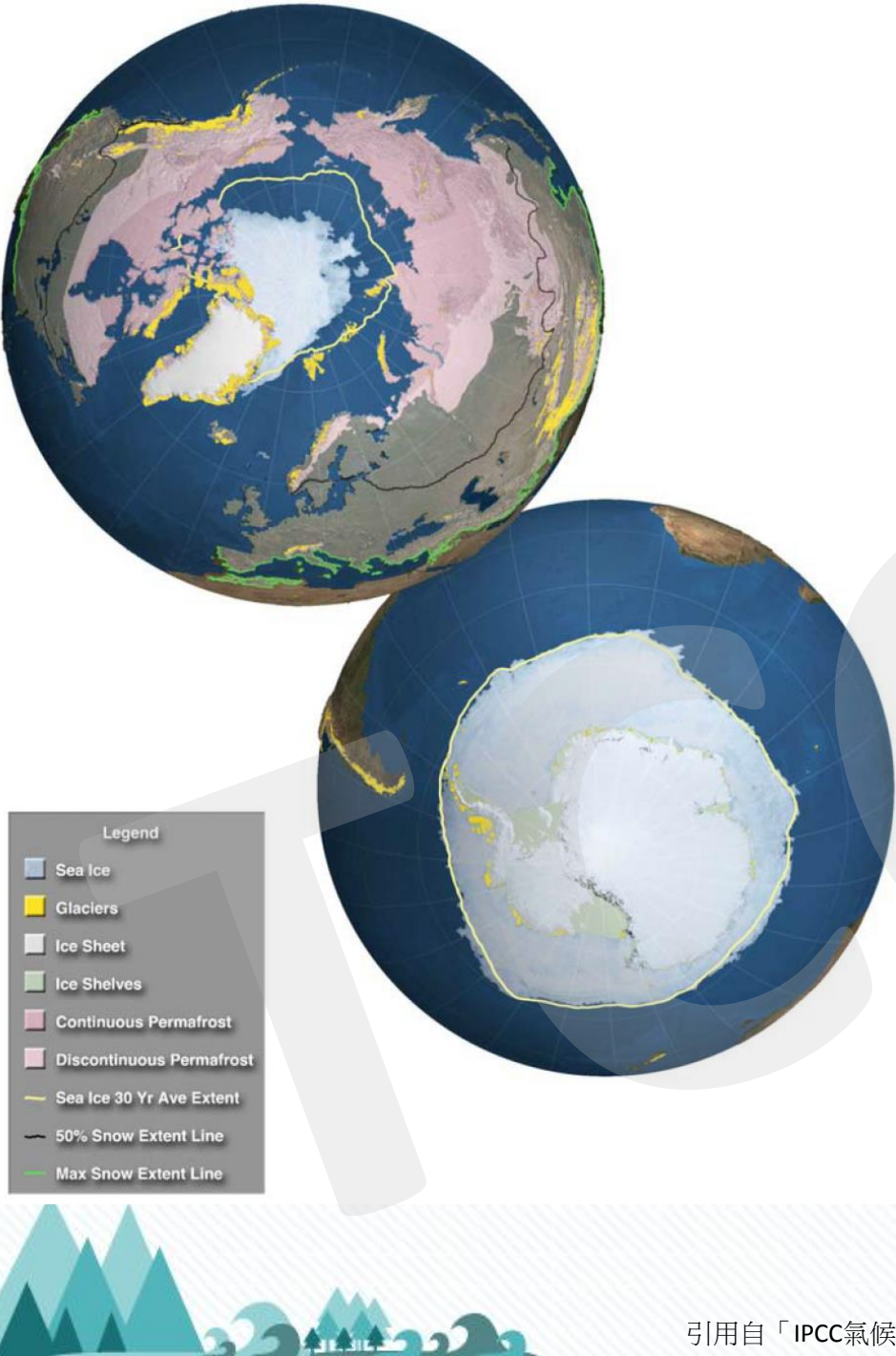
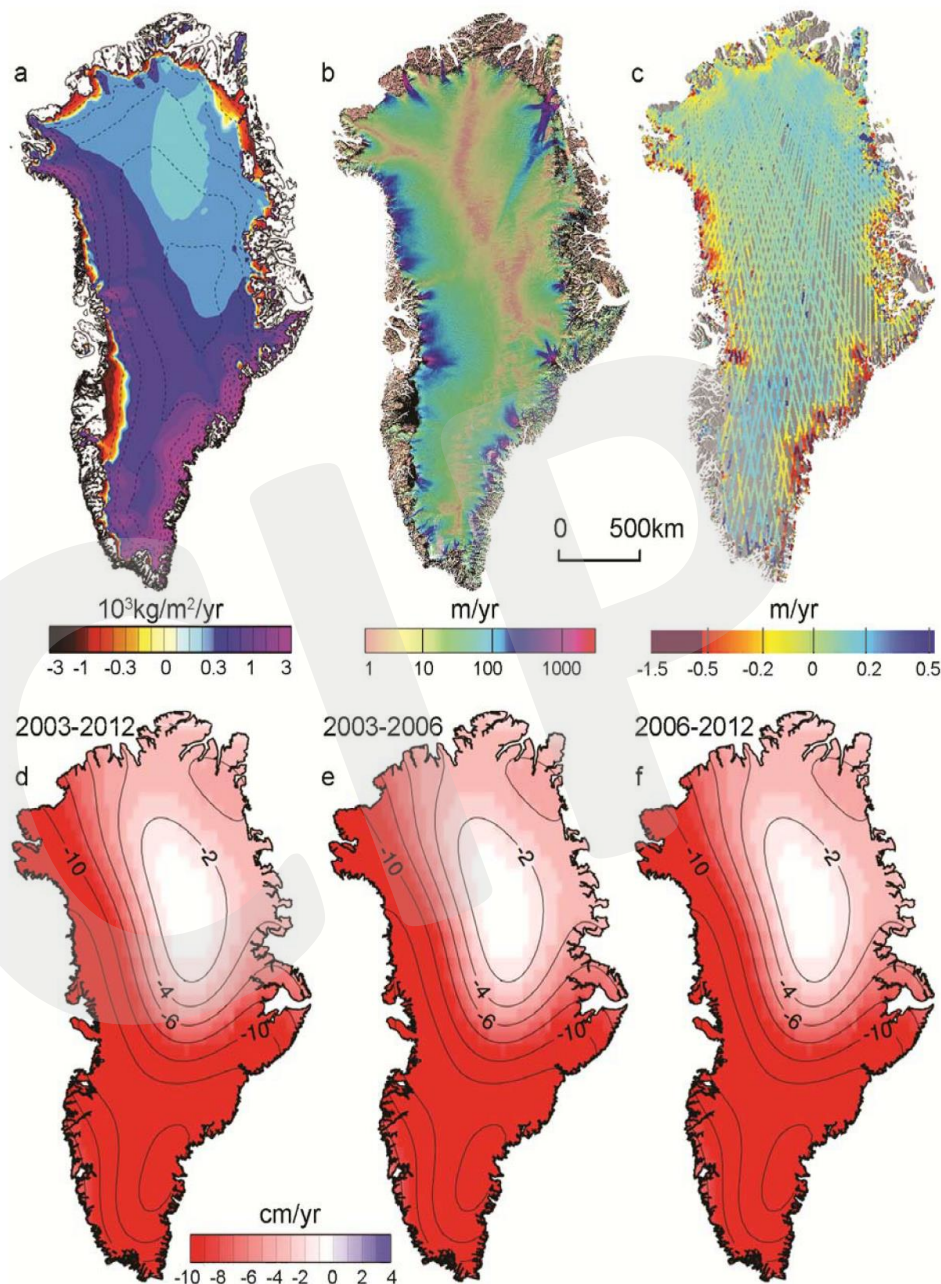


**Figure 4.1:** The cryosphere in the Northern and Southern Hemispheres in polar projection. The map of the Northern Hemisphere shows the sea ice cover during minimum summer extent (13th September 2012). The yellow line is the average location of the ice edge (15% ice concentration) for the yearly minima from 1979 to 2012. Areas of continuous permafrost (see Glossary) are shown in dark pink, discontinuous permafrost in light pink. The green line along the southern border of the map shows the maximum snow extent while the black line across North America, Europe and Asia shows the contour for the 50% snow extent. The Greenland ice sheet (blue/grey) and locations of glaciers (small golden dots) are also shown. The map of the Southern Hemisphere shows approximately the maximum sea ice cover during an austral winter (13th September 2012). The yellow line shows the average ice edge (15% ice concentration) during maximum extent of the sea ice cover from 1979 to 2012. Some of the elements (e.g., some glaciers and snow) located at low latitudes are not visible in this projection (see Figure 4.8). The source of the data for sea ice, permafrost, snow and ice sheet are datasets held at the National Snow and Ice Data Center (NSIDC), University of Colorado, on behalf of the North American Atlas, Instituto Nacional de Estadística, Geografía e Informática (Mexico), Natural Resources Canada, U.S. Geological Survey, Government of Canada, Canada Centre for Remote Sensing and The Atlas of Canada. Glacier locations were derived from the multiple datasets compiled in the Randolph Glacier Inventory (Arendt et al., 2012).

# 格陵蘭冰原的變化

**Figure 4.13:** Key variable related to the determination of the Greenland ice sheet mass changes. (a) mean surface mass balance for 1989–2004 from regional atmospheric climate modelling (Ettema et al., 2009); (b) ice sheet velocity for 2007–2009 determined from satellite data, showing fastest flow in red, fast flow in blue, and slower flow in green and yellow (Rignot and Mouginot, 2012); (c) changes in ice sheet surface elevation for 2003–2008 determined from ICESat altimetry, with elevation decrease in red to increase in blue (Pritchard et al., 2009). (d–e) Temporal evolution of ice loss determined from GRACE time-variable gravity, shown in centimetres of water per year for the periods (a) 2003–2012, (b) 2003–2006 and (c) 2006–2012, colour coded red (loss) to blue (gain) (Velicogna, 2009). Fields shown in (a) and (b) are used together with ice thickness (see Figure 4.18) in the mass budget method.



# 南極洲冰原的變化

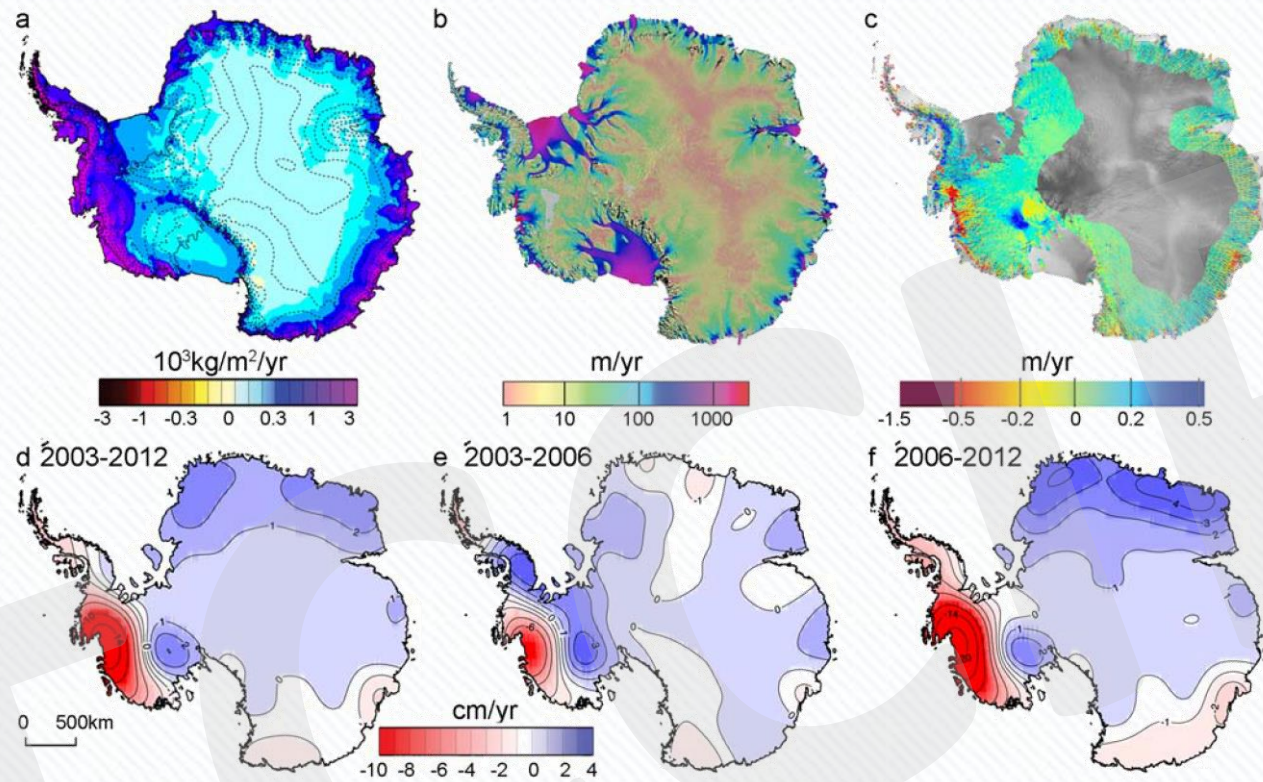


**Figure 4.14:** Key fields relating to the determination of Antarctica ice sheet mass changes. (a) mean surface mass balance for 1989–2004 from regional atmospheric climate modelling (van den Broeke et al., 2006); (b) ice sheet velocity for 2007–2009 determined from satellite data, showing fastest flow in red, fast flow in blue, and slower flow in green and yellow (Rignot et al., 2011a); (c) changes in ice sheet surface elevation for 2003–2008 determined from ICESat altimetry, with elevation decrease in red to increase in blue (Pritchard et al., 2009). (d-e) Temporal evolution of ice loss determined from GRACE time-variable gravity, shown in centimetres of water per year for the periods (a) 2003–2012, (b) 2003–2006 and (c) 2006–2012, colour coded red (loss) to blue (gain) (Velicogna, 2009). Fields shown in (a) and (b) are used together with ice thickness (see Figure 4.18) in the mass budget method.

# 陸冰溶化對海平面的影響

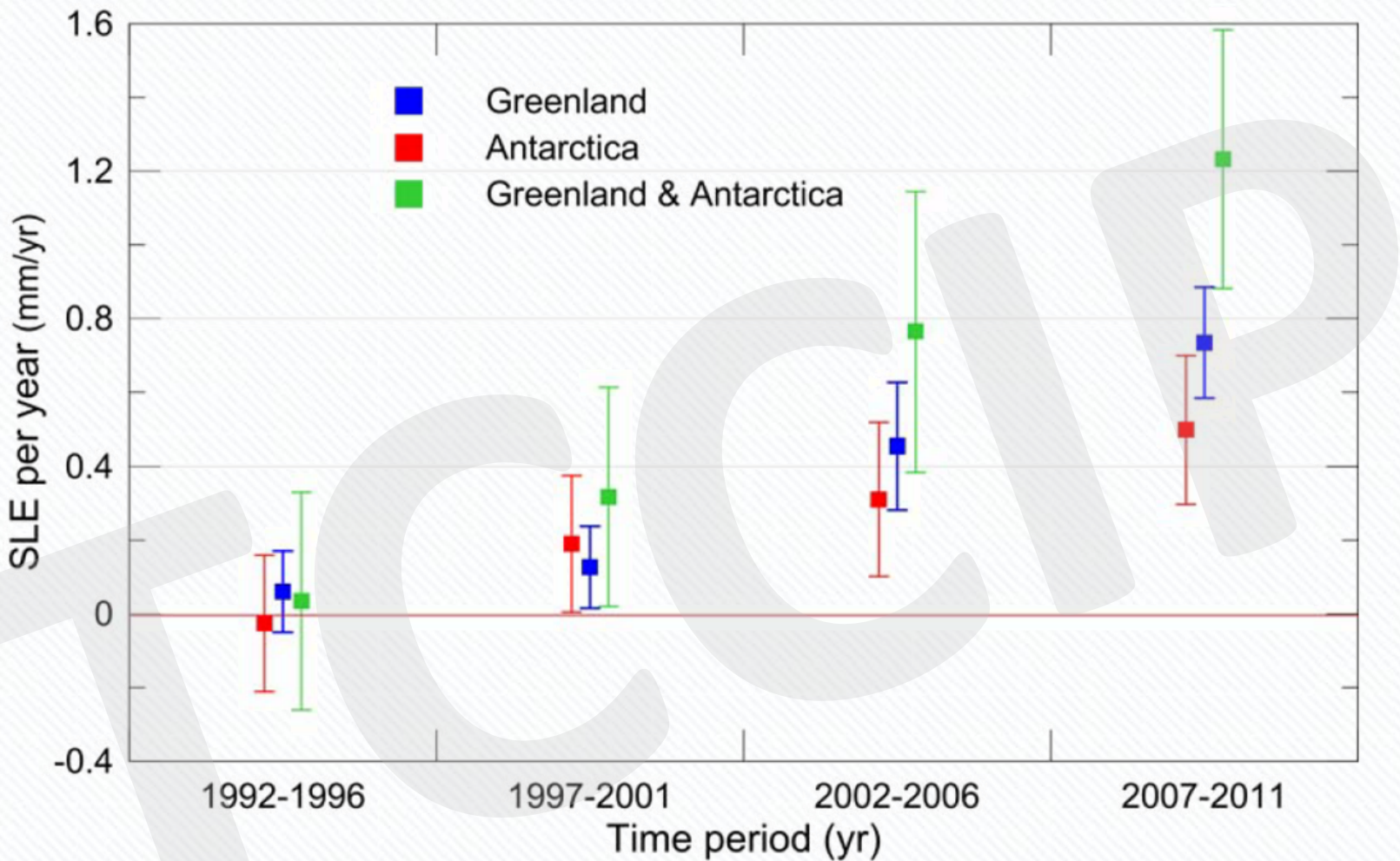
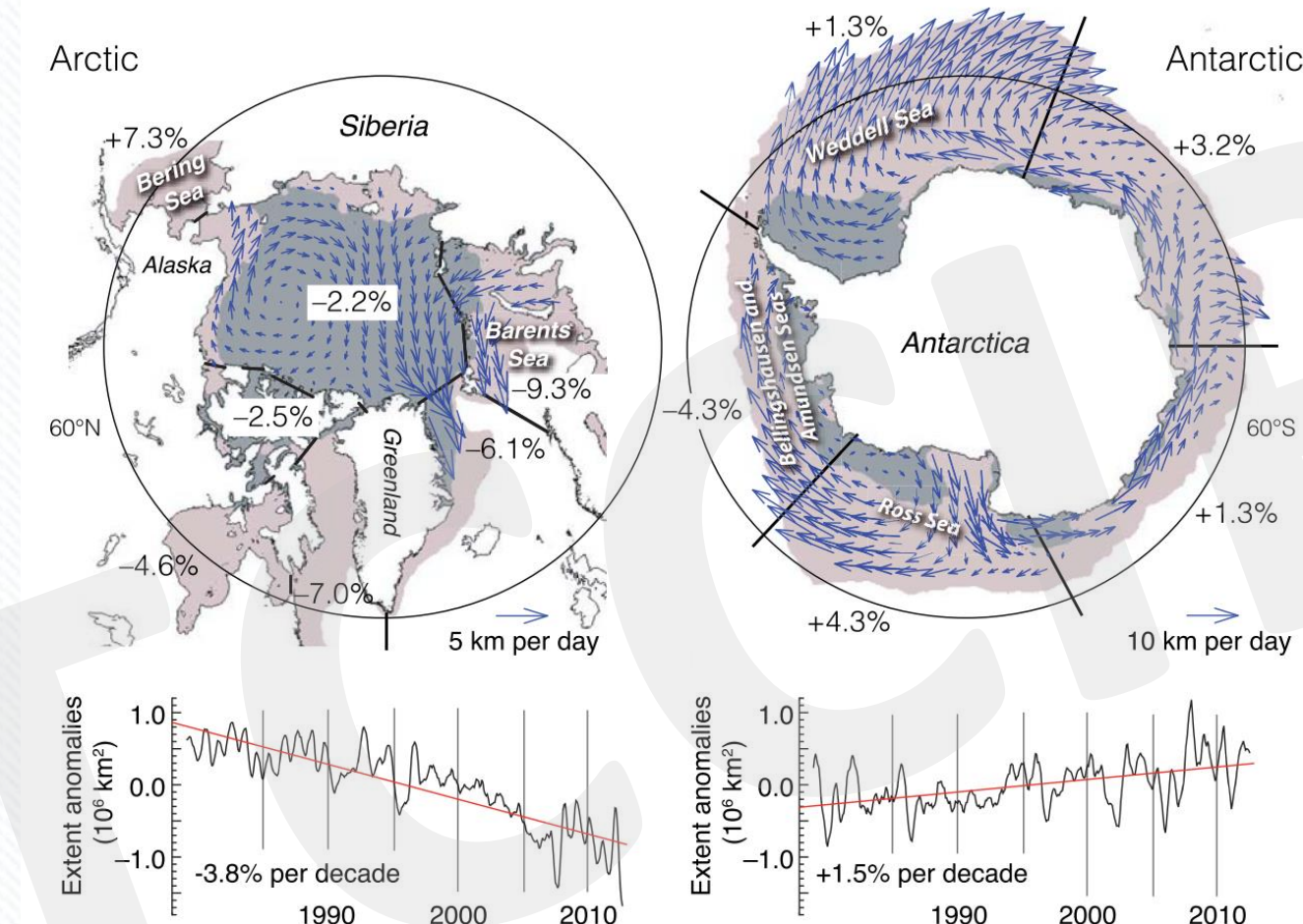


**Figure 4.17:** Rate of ice sheet loss in sea level equivalent averaged over 5-year periods between 1992 and 2011. These estimates are derived from the data in Figure 4.15 and Figure 4.16.

# 北極和南極海冰的變化



FAQ 4.2, Figure 1: The mean circulation pattern of sea ice and the decadal trends (%) in annual anomalies in ice extent (i.e., after removal of the seasonal cycle), in different sectors of the Arctic and Antarctic. Arrows show the average direction and magnitude of ice drift. The average sea ice cover for the period 1979 through 2012, from satellite observations, at maximum (minimum) extent is shown as orange (grey) shading.

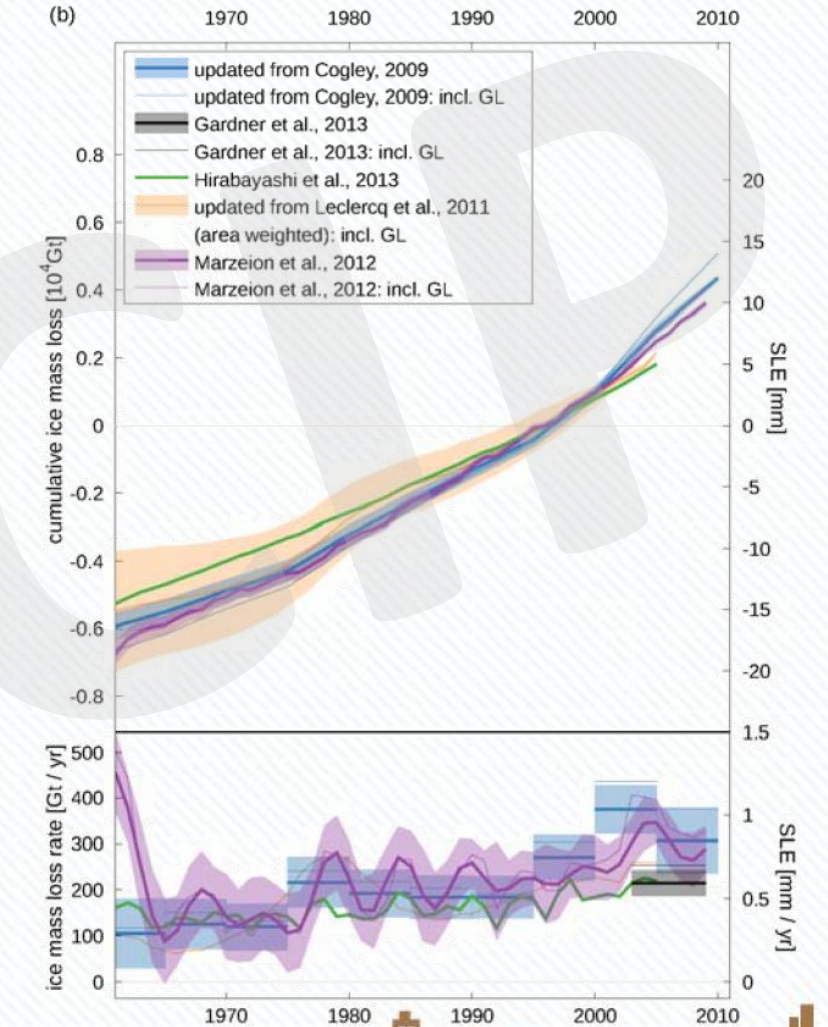
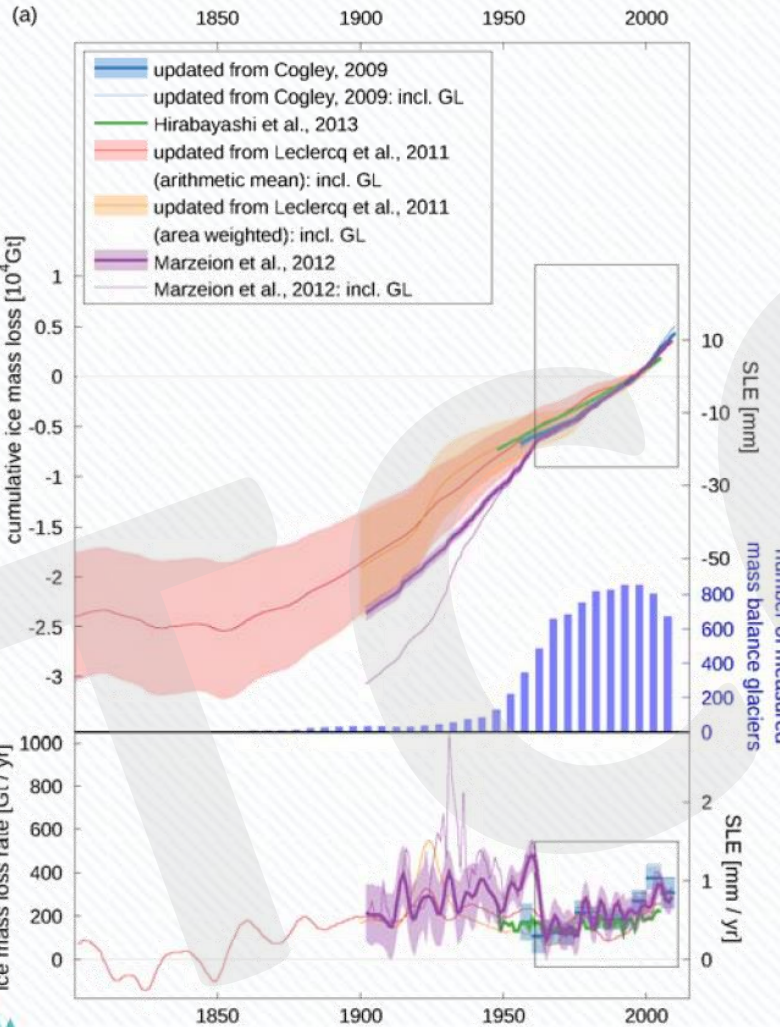
- ✿ 在1971至2009年間，世界各地平均的冰川冰量損失速率（不包括冰層外圍的冰川），非常可能 (very likely) 是 $226 [91-361]$  Gt yr $^{-1}$ ，在1993年至2009年間非常可能 (very likely) 達到 $275 [140-410]$  Gt yr $^{-1}$ 。
- ✿ 北半球的雪覆蓋範圍自二十世紀中期以來已經減少 (非常高可信度 very high confidence)。在1967到2012年間，北半球在三、四月份的雪覆蓋範圍每十年減少 $1.6 [0.8-2.4]$  %，六月的覆蓋範圍每十年減少 $11.7 [8.8-14.6]$  %。在這段期間，無論任何月份北半球的雪覆蓋範圍都未呈現達統計顯著性的增加。



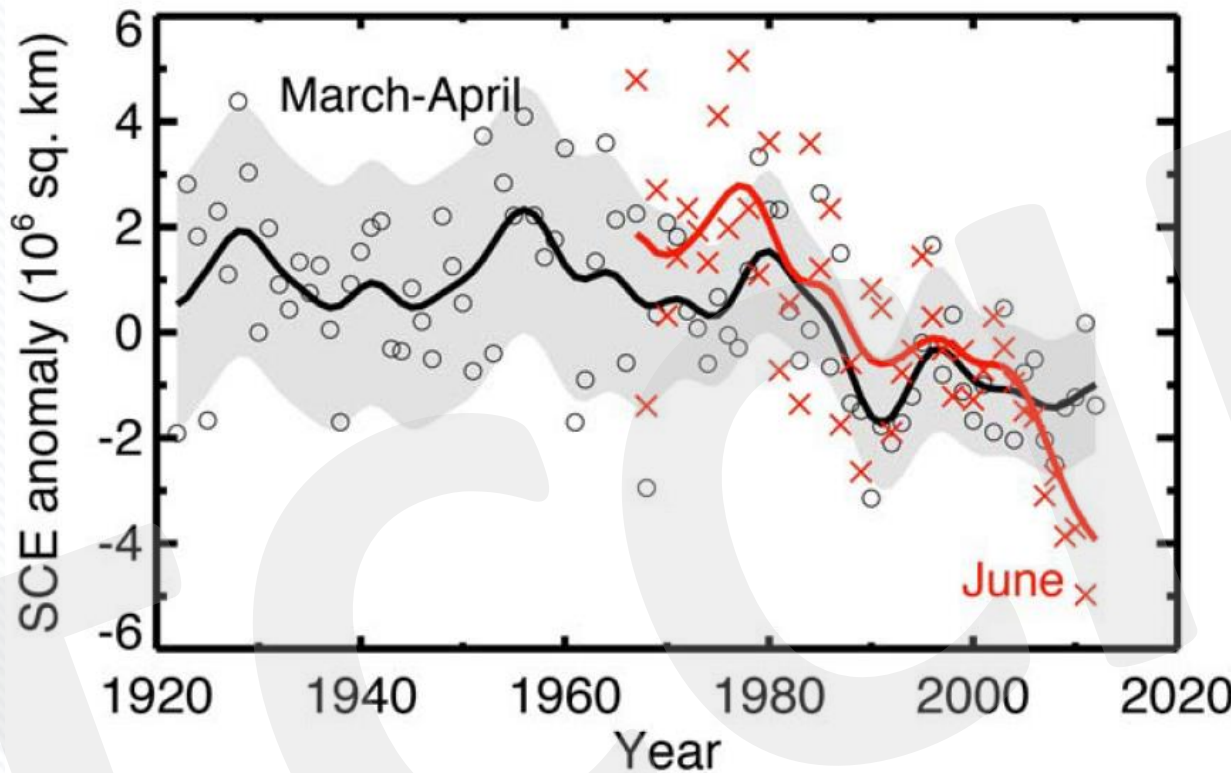
# 全球冰川質量

Figure 4.12:

Global cumulative (top graphs) and annual (lower graphs) glacier mass change for (a) 1801–2010 and (b) 1961–2010.



# 北半球三四月冰雪覆蓋面積的改變



**Figure 4.19:** March-April NH snow cover extent (SCE, circles) over the period of available data, filtered with a 13-term smoother and with shading indicating the 95% confidence interval; and June SCE (red crosses, from satellite data alone), also filtered with a 13-term smoother. The width of the smoothed 95% confidence interval is influenced by the interannual variability in SCE. Updated, from Brown and Robinson (2011). For both time series the anomalies are calculated relative to the 1971–2000 mean.

- ✿ 有高的可信度顯示，自1980年代初期起，大部分地區的永凍層溫度都已升高。在北阿拉斯加部分地區觀測到多達 $3^{\circ}\text{C}$ 的升溫（1980年代初期至20世紀中期），在歐洲北部的俄羅斯部分地區也觀測到多達 $2^{\circ}\text{C}$ 的升溫（1971至2010年）。在1975至2005年間，在後者亦觀測到永凍層厚度以及永凍層面積相當多的減少（中等可信度medium confidence）。

# 北半球凍土的變化

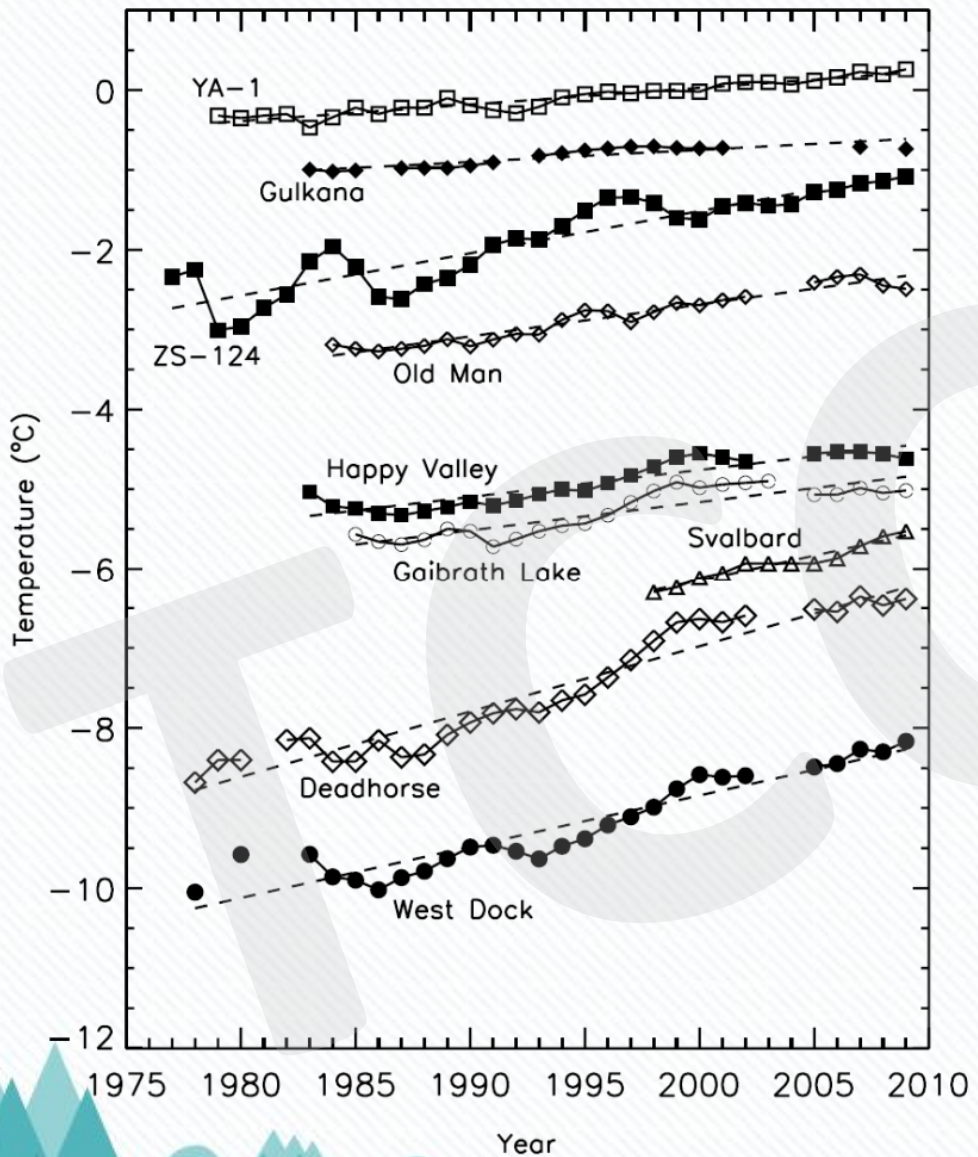


**Figure 4.22:** Time series of mean annual ground temperatures at depths between 10 and 20 m for boreholes throughout the circumpolar northern permafrost regions (Romanovsky et al., 2010a). Data sources are from Romanovsky et al. (2010b) and Christiansen et al. (2010). Measurement depth is 10m for Russian boreholes, 15 m for Gulkana and Oldman, and 20 m for all other boreholes. Borehole locations are: ZS-124 – 67.48°N 063.48°E; 85-8A – 61.68°N 121.18°W; Gulkana – 62.28°N 145.58°W; YA-1 – 67.58°N 64°E; Oldman – 66.48°N 150.68°W; Happy Valley – 69.18°N 148.88°W; Svalbard – 78.28°N 016.58°E; Deadhorse – 70.28°N 148.58°W; and West Dock – 70.48°N 148.58°W. The rate of change (°C/decade) in permafrost temperature over the period of each site record is: ZS-124:  $0.53 \pm 0.07$ ; YA-1:  $0.21 \pm 0.02$ ; West Dock:  $0.64 \pm 0.08$ ; Deadhorse:  $0.82 \pm 0.07$ ; Happy Valley:  $0.34 \pm 0.05$ ; Gaibrath Lake:  $0.35 \pm 0.07$ ; Gulkana:  $0.15 \pm 0.03$ ; Old Man:  $0.40 \pm 0.04$ ; and Svalbard:  $0.63 \pm 0.09$ . (The trends are very likely range, 90%)